We are IntechOpen, the world's leading publisher of Open Access books Built by scientists, for scientists

6,900
Open access books available

185,000
International authors and editors

200M
Downloads

Our authors are among the

154
Countries delivered to

TOP 1%
most cited scientists

12.2%
Contributors from top 500 universities



WEB OF SCIENCE™

Selection of our books indexed in the Book Citation Index in Web of Science™ Core Collection (BKCI)

Interested in publishing with us?
Contact book.department@intechopen.com

Numbers displayed above are based on latest data collected.
For more information visit www.intechopen.com



Chapter 11

Ion Acceleration by High Intensity Short Pulse Lasers

Emmanuel d'Humières

Additional information is available at the end of the chapter

http://dx.doi.org/10.5772/46137

1. Introduction

1.1. Context

Lasers can now deliver short and very intense pulses capable of producing hot and dense plasmas. The diffusion of such lasers has allowed studying the behaviour of ionized media in novel ways. Ion acceleration through laser plasma interaction is a recent research subject and its fast-paced progresses highlight the mastering of high power laser systems and the better understanding of the physics of high intensity laser plasma interaction. Short and intense laser pulses have also permitted the development of areas of research like harmonic generation, hard X-ray radiation sources, energetic particles sources and inertial confinement fusion. These researches have lead to numerous applications in transdisciplinary domains: material science, development of X-UV lasers, surface treatments, chemistry and biology are just a few examples. Large national programs are focused on these topics like the National Ignition Facility in California, the Laser Mégajoule and the Apollon laser in France.

These topics use plasmas where kinetic and collective effects are dominant with numerous non linear phenomena. Impressive progresses are being accomplished in the modelling of these phenomena and in their optimization thanks to Particle-In-Cell (PIC) codes. This is due to the fact that the mechanisms at play are complex and difficult to model analytically, or using a fluid model. PIC codes used to describe plasmas solve the coupled system of Maxwell's equations (for electromagnetic fields) and Vlasov equations (for each particle specie). The PIC method consists in solving Vlasov equation for each particle specie by the characteristics method for macro-particles, each representing a given amount of real particles but that conserves the mass and the charge of the particles of the specie that is studied. Several research areas of high intensity laser plasma interaction require PIC codes capable of modelling atomic physics processes (ionization and collisions for instance) and energy loss processes through radiation of energetic charged particles in intense electromagnetic fields.

INTECH
open science | open minds

© 2012 d'Humières, licensee InTech. This is an open access chapter distributed under the terms of the Creative Commons Attribution License (http://creativecommons.org/licenses/by/3.0), which permits unrestricted use, distribution, and reproduction in any medium, provided the original work is properly cited.

1.2. Ion acceleration in laser-plasma interaction

Particle accelerators play an important role in numerous scientific programs. Thanks to their versatility, they have found numerous applications in science and medical fields. Plasmas can endure very large acceleration gradients, making them very interesting as accelerating media. Particle acceleration by interaction of a high intensity laser with a gas or a solid is therefore attracting a growing interest. More and more laboratories in the world possess their own laser system and the results obtained by these laboratories, both theoretical and experimental, are very promising. It is nowadays possible to accelerate protons at energies of several tens of MeV [Snavely et al., 2000], and electrons at energies higher than a GeV [Leemans et al., 2006]. Moreover, the observation of intense energetic ion beams [M. Borghesi et al., 2006] represents one of the most interesting recent developments in "High Field Science", made possible by the advent of ultra-short and ultra-intense lasers [Mourou et al., 2006].

High power laser pulses open the possibility of ion acceleration to several tens MeV for protons, and higher than a GeV for Carbon ions on millimeter scale distances. These beams therefore open original perspectives, as new exploration tools of fundamental physics, or as new ways to increase the discovery potential of existing accelerators. Possible applications of these beams are numerous: ion fast ignition for inertial confinement fusion (in which a "spark", a beam of energetic ions, is used to ignite a target and reduces the total energy cost), high resolution radiography of plasmas, hadrontherapy, radio-isotopes production, laboratory astrophysics, etc… Indeed, the properties, not explored until now, in terms of current, duration (of the order of a few ps), laminarity (low divergence) and compactness – the acceleration process takes place on a distance of the order of ten microns – show that these beams are complementary, and even superior on some aspects to conventional accelerators. Finally, the constant development of high intensity lasers, on the duration, energy, repetition rates, and compactness aspects, makes the applicability perspectives of these intense sources extremely promising.

The maximum energy, as well as the properties of these ion/proton beams go well beyond the limits explored during the first experiments performed at the end of the seventies that observed ion beams from laser-matter interaction. In these first experiments, targets were irradiated with CO_2 (λ=10,6 μm) lasers with pulse durations < 1 ns and peak intensities $I\lambda^2$ of the order of 10^{17}-10^{18} W.cm^{-2}.μm^{-2} [Begay et al., 1982]. The ions were emitted from the surface of the target irradiated by the laser, with a large angular divergence and an energy of a few 100 keV/nucleon. The protons originated from contaminants on the target surface. These experiments, repeated using Nd:Glass lasers at λ=1 μm produced similar results, with a higher ion energy due to the increased $I\lambda^2$ [Fews et al., 1994; Clark et al., 2000b] . Simulations using the parameters of these experiments showed that the ion acceleration process could in this case be described as a plasma expansion in vacuum mechanism, first considered isothermal [Gitomer et al., 1986; Sack et al., 1987], or adiabatic.

The discovery of energetic and collimated ion beams was made thanks to a recent fortuitous observation. The related experimental results were published in 2000 and obtained on the

LLNL PetaWatt system in the USA. The scientists conducting the experiments wanted to study the electron beams generated during the interaction of this laser with solid targets. From these first experiments using short pulses (ps) [Clark et al., 2000a; Snavely et al., 2000; Maksimchuk et al., 2000], it therefore appeared that these ion beams presented extremely interesting characteristics. Since, many experiments helped to understand the physics of laser ion acceleration with solid targets, and showed that this source possesses unique characteristics in comparison to beams produced using conventional accelerators:

- Excellent transverse laminarity (more than 100 times better than conventional accelerators [Borghesi et al., 2004; Cowan et al., 2004]).
- Extremely small equivalent source size (μm), characteristic equivalent to the laminarity that allows to obtain an excellent spatial resolution for radiography applications [Borghesi et al., 2002; Mackinnon et al., 2004].
- Very short duration of the source (~ps), allowing to obtain an excellent temporal resolution for pump/probe applications.
- Large energy spectrum (which can be modulated [Hegelich et al., 2006; Schwoerer et al., 2006; Toncian et al., 2006], as can be modulated the divergence [Patel et al., 2004; Toncian et al., 2006]), allowing to obtain in a single radiography, through the different associated times of flight, a movie of the probed phenomena in a single shot.
- Very high current at the source ~kA.
- Intrisic compactness of the acceleration, from 0 to a few tens MeV in a few ten microns (the compactness of the whole "accelerator" is therefore linked to the one of the laser).

It was demonstrated by studying the acceleration physics that the energetic ions observed were accelerated electrostatically from the non-irradiated surface, by fast electrons generated in the interaction zone between the ultra-intense laser and the target, and propagated through the target, as originally predicted [Hatchett et al., 2000; Wilks et al., 2001]. It was also demonstrated that the divergence parameters or the ion energy distribution could be changed using micro-setups triggered by ultra-short lasers [Toncian et al., 2006].

These studies on the understanding of the properties of laser accelerated ion beams have opened original application perspectives in various domains, for fundamental research (study of warm dense matter) and the development of diagnostics for ICF (Inertial Confinement Fusion), as well as for possible medical applications, extremely motivating even if their effective realization is still uncertain (protontherapy for instance):

- Plasma diagnostics for inertial fusion with lasers (analysis of rapidly evolving electric and magnetic fields), analysis of dense objects (static and dynamic like in the case of the compression of a fusion capsule) with resolutions ~ps and ~μm, or for the ignition [Roth et al., 2001; Atzeni et al., 2002; Temporal et al., 2002; Temporal, 2006; Key et al., 2006] of fusion reaction for ICF [Tabak et al., 1994].
- Production of large scale hot and dense plasmas [Patel et al., 2004; Antici et al., 2006], an important aspect for the study of equation of states.
- Injection in conventional accelerators [Krushelnick et al., 2000a; Cowan et al., 2002, Antici et al. 2008b] and evaluation of the potential of laser-accelerated protons for

medical applications (protontherapy [Bulanov et al., 2002a; Bulanov et al., 2002b; Fourkal et al., 2002; Malka et al., 2004] or production of radio-isotopes [Santala et al., 2001; Fritzler et al., 2003; Ledingham et al., 2004; Lefebvre et al. 2006]).

Recently (in 2011), two teams of experimentalists from the Los Alamos National Laboratory beat the maximum laser accelerated ion energy world records one after the other, obtaining 80 MeV and then 120 MeV for protons and Carbon ions with energies higher than a GeV with a 130 TW laser system and an intensity of a few 10^{20} W/cm^2. The main laser ion acceleration mechanisms are now known and understood, the acceleration by hot electrons (or Target Normal Sheath Acceleration, TNSA), and the acceleration by radiation pressure, but new regimes are explored and an important theoretical and experimental effort is ongoing to further our understanding of laser ion acceleration with various types of targets, to understand its limits in the high laser intensity and in the high laser energy regimes, and to get closer to some applications (Fast Ignition, hadrontherapy…).

Section 2 of this Chapter will present laser ion acceleration with flat dense targets, both through plasma expansion and through the laser radiation pressure with some details on the particular case of circularly polarized laser pulses. The transparency regime is also discussed. Section 3 is devoted to laser ion acceleration using low density targets, either gas jets, exploded foils or foams. Section 4 is devoted to laser ion acceleration using structured targets like cones or reduced mass targets to improve specific characteristics. Section 5 is devoted to the ultra high laser intensity and ultra high laser energy regimes that are starting to be accessible with recent laser systems and that will be further explored in the near future with laser systems under construction. Section 6 is devoted to the presentation of several applications of laser ion acceleration and Section 7 presents the conclusions and perspectives of this Chapter.

2. Laser ion acceleration with flat dense targets

Laser ion acceleration using flat solid foils has been the subject of numerous studies in the last ten years, experimental, theoretical and numerical. This Section presents some important results obtained in these studies. First, results on the TNSA regime are presented with the main scaling laws for the maximum proton energy in this regime. Laser ion acceleration through the laser radiation pressure is then introduced with its extension to circularly polarized laser pulses. Both recent theoretical results and first experimental demonstrations are discussed. The special case of the transparency regime is then presented allowing a coupling of the TNSA and of the radiation pressure regime.

When a high intensity laser (>10^{18} W/cm^2) with a short pulse duration (30 fs – 10 ps) irradiates a target, this pulse produces, at the effective critical density (~10^{21} cm^{-3}), where the laser pulse can not penetrate the plasma, a population of "fast" electrons through different mechanisms (acceleration by the ponderomotive potential [Wilks et al., 1992], resonant absorption [Estabrook et al. 1978], the Brunel effect [Brunel, 1987], mechanisms

that are not the primary goal of this Chapter). The dominant mechanism accelerating the electrons depends on the gradient on the front surface and on the laser incidence angle [Lefebvre et al., 1997]; moreover, depending on the interaction conditions, the electrons are accelerated, either in the laser direction, or in the target perpendicular direction [Santala et al., 2000].

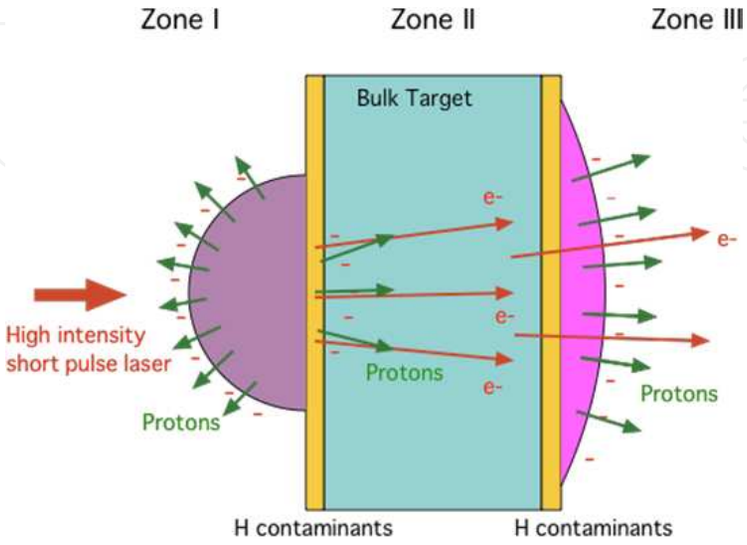


Figure 1. Illustration of the various mechanisms leading to high energy ion acceleration by a short and high power laser interacting on a solid target.

In zones I and III (Figure 1), the mechanism is a plasma expansion, with at its front a Debye sheath of hot electrons. In zone III, where there is no initial gradient (in zone I, it is possible only by using very high temporal contrast lasers, which has only been possible recently [Ceccotti et al., 2007]), there is an important difference with zone I: initially, the situation is the one of a virtual cathode where electrons partially extend in vacuum whereas atoms remain structured on the target surface. This is the origin of the high quality of the beam. Following this initial phase, the electrons steadily transfer their energy to the ions and the charge separation field associated to the electron sheath gradually decreases until the acceleration stops, when the electrons are at the same velocity as the ions. This results in the existence of a "cutoff" energy, i.e. a maximum energy of the ion beam, already observed in the seventies. In zone II, protons are accelerated by the strong electrostatic field set up when the laser pulse pushes electrons inside the target.

Except the energy reached by the ions, the main difference between the accelerations in zone I and II on one hand and III on the other hand is that one develops from a pre-existing plasma while the other one originates from an initially cold surface, unperturbed. Therefore, acceleration in zone I or II produces a beam largely divergent (2π sr) and turbulent (the structure of the ion front is thermal, not ordered) while acceleration in zone III produces a beam with a limited divergence (determined by the spatial structure of the hot electron sheath), and especially, extremely laminar thanks to the structure of the back surface (if it has a good surface quality) [Fuchs et al., 2005; Fuchs et al., 2007a].

2.1. The target normal sheath acceleration

The production of energetic electrons when a high intensity laser interacts with a solid foil has been explained above. These electrons are going to form a hot electron cloud around the target leading to a plasma expansion on both sides of the target [Wilks et al., 2001]. The resulting electrostatic field will then accelerate ions located on both sides of the target to high energies. The amplitude of this field (~TV/m) depends on the hot electron temperature and density. Protons can also be accelerated if they are present in the target or on its surface as contaminants. The basics of the theory of hot plasma expansion [Mora, 2003; Mora, 2005] will be presented and their use in obtaining scaling laws for the maximum proton energy will be explained [Fuchs et al., 2006a; Fuchs et al., 2007a, Robson et al., 2007]. This regime is the so-called "Target Normal Sheath Acceleration" regime (TNSA).

The space charge fields in zones I and III are evidently determined by the local electron density and by the extension of the charge separation [Hatchett et al., 2000; Wilks et al., 2001]. The separation length between electrons and ions is given either by the Debye length (λ_D~1 μm for 1 MeV electrons), either by the local gradient length (notably for the part on the front of the target) if it is greater than λ_D [Fuchs et al., 2007b]. As in most cases the laser pulse has a pedestal, a plasma is generated at the front surface and therefore the field is in general lower in zone I than in zone III, which confirms the experimental measurements: the energy of ions accelerated towards the laser (in zone I) is smaller than the energy of the ions accelerated in the same direction as the laser propagation direction (in zone II or III) [Ledingham et al., 2004; Yang et al., 2004]. Thanks to the density and temperature of electrons in zone III, and to the value of λ_D, the field in zone III is initially of the order of a few TV/m.

Acceleration in zone III is the most suited to produce a high quality beam, laminar, that is adapted to imaging applications. Because of the high energy required for electrons to reach zone III, this mechanism was only made possible by the advent of high power laser with short pulse durations. This mechanism also produces, with nowadays lasers, more energetic ions than the acceleration in zone II. The respective energy that can be reached by the accelerated protons in the three zones is illustrated in [J. Fuchs et al., 2007a]. Acceleration in zone II produces less energetic protons for different laser/target conditions as confirmed by PIC simulations performed in a wide range of parameters (for laser intensities going from 10^{17} to 5×10^{19} W/cm^2, and for laser pulse duration ranging from 10 fs to 500 fs) [Sentoku et al., 2003; Murakami et al., 2001; Pommier et al., 2003; Pukhov, 2001]. It is also noteworthy that the acceleration in zone II produces a beam with a lower quality [Fuchs et al., 2005] due to the stochastic nature of laser-plasma interaction (in the preplasma) which does not produce a charge separation field structure at the critical density interface as ordered as the one existing at the back (non perturbed) surface of the target (zone III). The collimation and low emittance of rear side accelerated ions are considerable assets for numerous applications.

Nevertheless, we can note that the use of high temporal contrast lasers will erase the differences between the acceleration in zones I and III: in these conditions, there will be no

preplasma, and therefore the spatial quality of the ion beams produced in zones I and III will be similar [Ceccotti et al., 2007]. If the target is, in addition, very thin, the electron populations will be similar on both sides of the target and the ion energy will therefore also be very close. On the contrary, for thick targets, the electrons will have a lower density when arriving at the back surface of the target (zone III), and the resulting accelerating field as well as the maximum ion energy will thus be lower in this zone than in zone I.

An acceleration model has been developed to obtain a predictive model of maximum ion energy useful for experimentalists [Fuchs et al., 2006; d'Humieres et al, 2006; Fuchs et al., 2007a]. This model uses theoretical results on the isothermal expansion of a hot plasma [Mora, 2003] coupled to a model of characteristic ion acceleration time. By studying the dependence of this characteristic time on various parameters, it was possible to extend the validity of this model to very short pulse durations.

This study has also allowed to link the characteristics of the TNSA accelerated ion beams to the characteristics of the energetic electron population in order to develop a new diagnostic of this electron population for laser-plasma interaction experiments [Antici et al., 2008a].

To obtain an analytical estimate of the maximum energy that can be gained by protons accelerated forward from the back surface of the target (zone III) [Fuchs et al., 2006; d'Humieres et al, 2006; Fuchs et al., 2007a] it is possible to use the approach chosen by Mora [2003], which was based on an approach initiated in the seventies to treat the expansion of a plasma in vacuum, and adapted to the case of a hot electron burst initiating the expansion. In the case of a self-similar isothermal expansion [Gurevitch et al., 1966], a simple evaluation of the accelerated ions maximum energy is:

$$E_{max/back}=2ZT_{hot}*[\ln(t_p+(t_p^2+1)^{1/2})]^2$$

Where T_{hot} is the electron temperature in the sheath in zone III and $t_p=\omega_{pi}*t_{acc}/(2*\exp[1])^{1/2}$ with t_{acc} the acceleration time and $\omega_{pi}=\sqrt{\frac{n_{e0}Ze^2}{M_i\varepsilon_0}}$ the ion plasma frequency (n_{e0} is the initial electron sheath density at the back of the target and M_i the ion mass). As already mentioned, in most experiments, a plasma is located on the front surface during the target irradiation by the main pulse. In this case, as already showed in experiments, T_{hot} can be well approximated using the ponderomotive potential $m_ec^2(\gamma-1)$ [Malka et al., 1996; Popescu et al., 2005]. In reality the expansion is far from being isothermal, and is actually adiabatic [P. Mora, 2005]. Starting from a hot electron cloud, there is a progressive energy transfer through the electrostatic fields to the ions. Nevertheless, such an adiabatic model cannot be solved analytically, only numerically.

The ambition of this model was to see if the isothermal model could be used, having the advantage of being simple and easy to use analytically, by compensating with a finite (determined) acceleration time the fact that the hot electron population is maintained at a constant temperature [Fuchs et al., 2006]. To confront this approach with experimental

results and see how interesting it is, it is important to determine the missing ingredients, namely n_{e0} and t_{acc}.

To determine n_{e0}, the quantity of hot electrons accelerated inside the target by the laser has been evaluated in a simplified way, with an energy balance. This quantity can be evaluated as $N_e = f\,E/T_{hot}$, where f is the laser energy fraction absorbed in the plasma and converted in hot electrons. This fraction f was measured by using a buried layer inside the targets and by measuring the X-ray radiation induced in these layers by the hot electrons. This way, it is possible to determine the total energy in the hot electrons and therefore f. It depends of the incident laser intensity: $f = 1.2\times10^{-15} I^{0.74}$ (where I is in W/cm^2 units) with a maximum f of 0.5. We can now assume that these electrons are, longitudinally, confined and transversally diluted in the target [Kaluza et al., 2004] until they are spread on the electron sheath area A_{sheath} at the back of the target. This would give $n_{e0}=N_e/(d\times A_{sheath})$ where $A_{sheath}=\pi(r_0+d\times\tan\theta)^2$, d is the initial target thickness and r_0 is the radius of the zone from which the electrons are accelerated at the critical interface, radius that we assume to be equal to the focal spot radius (r_0=FWHM). A_{sheath} also depends on the hot electron divergence half-angle in the target θ. Several experimental and theoretical studies show that θ is between 15° and 40° [Fuchs et al., 2003; Stephens et al., 2004; Adam et al., 2006], increasing with laser energy [Lancaster et al., 2007; d'Humières et al., 2006].

In the model, θ=25° has been chosen in agreement with what the LULI team had deduced from astigmatic proton emission measures [J. Fuchs et al., 2003]. This model is supported by the fact that:

- The values of the size of the electron sheath at the back of the target obtained with this model are in good agreement with direct measures that can be obtained of the size of the proton source.
- The values of electron density at the back of the target as well as the ones of the zone on which these electrons spread are also in good agreement with direct measures of these parameters performed using an interferometry diagnostic with a probe beam reflected on the back of the target that was adapted to this problem [Antici et al., 2008a].

To determine the accelerating time t_{acc}, different approaches were tested by comparing them not only to data obtained during experiments for laser intensities ranging from 2×10^{18} to 6×10^{19} W/cm^2, and for laser pulse durations between 150 fs to 10 ps [Fuchs et al., 2006], but also to data obtained with shorter pulse durations taken from various articles. A priori, one could think that t_{acc}, which represents physically the time during which in the model the electron temperature is maintained to T_{hot} must be proportional to the laser pulse duration. Nevertheless, for very short pulse durations, it is important to take into account a minimum time for the energy transfer between electrons and ions. Therefore, for very short pulse durations, the acceleration time is not proportional to the laser pulse duration anymore but needs to tend towards a constant value. It is also necessary to include in the model the fact that this acceleration time needs to depend on the laser intensity. Indeed, for low laser intensities, this acceleration time needs to be increased because the expansion is slower. In

the end, the function, which is most adapted to the different experimental measures, is [J. Fuchs et al., 2007a]: $t_{acc}=\alpha*(\tau_L+t_{min})$ where τ_L is the laser pulse duration, t_{min}=60 fs and where α goes linearly from 3 for an intensity of 2×10^{18} W/cm² to 1.3 at 10^{19} W/cm² and is constant at 1.3 for higher intensities. The figures in [Fuchs et al., 2006; d'Humières et al., 2006], as well as Figure 2 show a comparison between the calculations of the maximum proton energy $E_{max/back}$ and experimental results obtained in a wide range of laser and target parameters (in particular for short pulse durations, and/or low intensities that were not explored experimentally at LULI). This model was also validated using 2D PIC simulations [d'Humières et al., 2006].

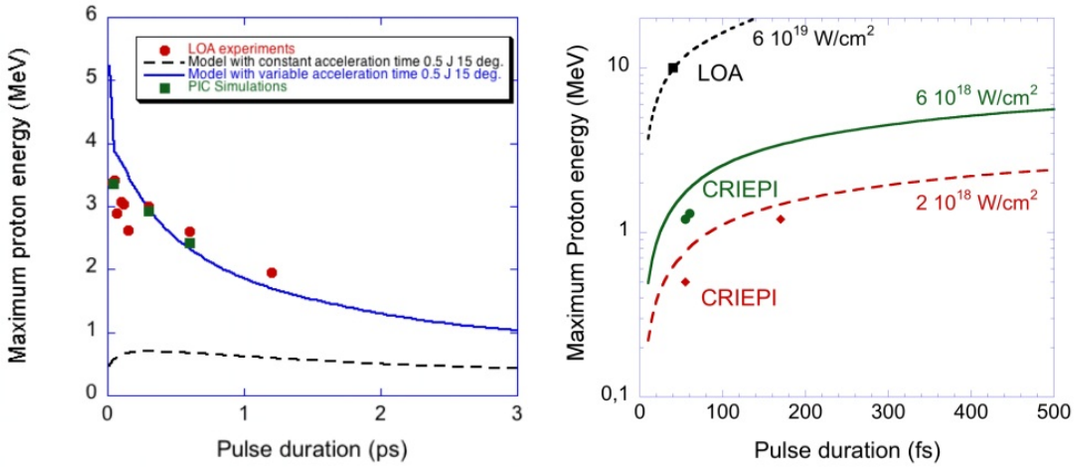


Figure 2. (Left) Data (points), simulations (squares) and model (lines) giving the maximum proton energy as a function of the pulse duration for very short pulse durations. In the model, a focal spot of 6 μm FWHM is used as well as a target thickness of 5 μm. The different lines correspond to different intensities for which the experiments were performed. (Right) Same graph but for various laser systems (points) and the model (lines). Here a thickness of 5 μm was used in the model as most of the reported experiments used a similar thickness.

It is nevertheless important to keep in mind that the acceleration time t_{acc} is not the « true » acceleration time, it is the typical time during which the electron population remains at a « high » temperature. In reality, the hot electron temperature decreases progressively during the energy transfer between electrons and ions.

To conclude this Section, the analytical work on the maximum proton energy produced with the accelerating mechanism in zone III has allowed to obtain an evaluation tool that is able to correctly reproduce the existing data obtained at LULI and other laser systems, and to extrapolate it to other laser parameters (it is important to keep in mind that this model can only be entirely reliable in the parameter range in which it has been tested).

Effects of a small scale gradient at the back of the target on laser ion acceleration in this regime has also been investigated [Fuchs et al., 2007b], and the physics of long pulse interaction and its effects on the creation of the accelerating electron sheath is now being intensely studied.

2.2. Laser ion acceleration through the laser radiation pressure

Laser ion acceleration through the laser radiation pressure has first been studied theoretically and using Particle-In-Cell simulations by Wilks et al. [1992] and Denavit et al. [1992]. It was first referred as the hole boring regime and can lead to the development of strong electrostatic shocks inside the target [Silva et al., 2004]. Electrons are pushed by the laser ponderomotive force at the front of the target and lead to a strong charge separation setting up a high amplitude electrostatic field. This field will accelerate front surface ions to high energies during the duration of the laser pulse. This regime is also referred to as Radiation Pressure Acceleration (RPA) or the laser piston regime.

It is possible to estimate analytically the maximum proton energy of forward accelerated protons from the front surface. Indeed, the maximum velocity of the accelerated protons in zone II is given by two times the receding plasma surface velocity [Pukhov, 2001; Denavit, 1992]. In the case of a total laser reflection at the critical interface (i.e. when the laser piston efficiency is maximum), this receding velocity is given by [Wilks et al., 1992; Wilks, 1993] :

$$\frac{u_s}{c} = \sqrt{\frac{1}{2}\frac{n_c}{n_e}\frac{Zm_e}{M_i}a_0^2}$$

Where n_c is the effective critical density, where the laser wave reflection takes place, i.e. $n_e=\gamma n_c$ [Fuchs et al., 1999] at normal incidence with γ being the Lorentz factor given by $\gamma=(1+a_0^2)^{1/2}$, with $a_0^2=(p_{osc}/mc)^2=I\lambda^2/(1.37\times10^{18})$, I being the laser intensity (in units of W/cm^2) and λ is the laser wavelength in microns.

Therefore:

$$E_{max/front} = 2*M_i*u_s^2=Zm_ec^2a_0^2/\gamma$$

One can note that this evaluation is consistent with the values measured specifically for protons produced in zone II [Kaluza et al., 2004] that can indeed be measured using two different techniques:

- With neutron spectroscopy: by using a CD_2 target and by measuring the emitted neutrons [Youssef et al., 2006; Habara et al., 2004].
- With nuclear activation [Nemoto et al., 2001]: a thin layer containing Deuterium is placed at the front of Al targets. Experimentalists were able to quantitatively determine the D^+ spectrum emitted in zone II for which the maximum cutoff energy compared favourably with the formula above [Fuchs et al., 2005; Fuchs et al., 2007a].

The analytical work on the maximum proton energy produced with the accelerating mechanism in zone II has allowed showing that the acceleration mechanism in zone III produces, in almost every case, the maximum proton energies [Fuchs et al., 2007a].

This conclusion can be obtained using four different means:

- First, experimentally, it was possible to demonstrate that acceleration in zone III produces the forward accelerated protons with the maximum energy.

- Then, the same conclusion related to the fact that acceleration in zone III is dominant can be reached by observing the agreement between the experimental measures and the predictions of the acceleration model in zone III (see above).
- The models described in this Section and in Section 2.1 are also in good agreement with 2D PIC simulations over a wide range of target and laser parameters.
- Finally, when comparing systematically the maximum proton energies obtained by the two mechanisms, one also notes the dominance of acceleration in zone III to generate the most energetic protons. This comparison was done for various pulse durations, target thicknesses and laser intensities [Fuchs et al., 2007a]. The dominance of zone III is systematic, except for ultra-short pulse durations (< 10 fs) for which the laser energy is too low and the number of electrons accelerated towards the back surface is therefore low, thus reducing the amplitude of the accelerating field at the back of the target.

With this study, the controversy on the origin of the most energetic protons was concluded.

More recently, this regime has been revisited in the case of a circularly polarized laser pulse. In this case, a strong electrostatic field is also created at the front of the target as electrons are pushed forward but they are not heated. They therefore create a thin electron layer travelling inside the target. The hot electron temperature and density are therefore decreased, also decreasing the efficiency of the TNSA mechanism. The thin accelerated electron layer will drive a strong charge separation that can lead to the acceleration of quasi-mono-energetic ion beams. Recent numerical and theoretical studies [Klimo et al., 2008; Robinson et al., 2008; Macchi et al., 2009; Grech et al., 2011; Schlegel et al., 2009; Tamburini et al., 2010], as well as recent experimental studies [Henig et al., 2009] have explored this regime. It can also be explored using higher wavelength with CO_2 lasers interacting on gas jets [Palmer et al., 2011; Haberberger et al., 2011].

2.3. Laser ion acceleration in the transparency regime

A new regime of laser ion acceleration which relies on the interaction of high contrast laser pulses with ultra thin foils has been validated using simulations [Dong et al. 2003; d'Humières et al., 2005; Yin et al., 2006; Albright et al., 2007] and experiments [P. Antici et al., 2007; D. Neely et al., 2006]. In this regime, the laser is able to go through the target during the duration of its interaction. Both the TNSA mechanism and the radiation pressure acceleration can play an important role in this case and laser energy absorption is increased as volume absorption occurs.

It has been shown that proton energy could be increased by reducing the solid target thickness [Mackinnon et al, 2002; Kaluza et al., 2004]. For extremely thin targets where relativistic transparency for the laser pulse occurs, theoretical studies [Dong et al., 2003; d'Humières et al., 2005; Esirkepov et al., 2006; Yin et al., 2006] have suggested that proton acceleration could be even more efficient than using the standard regime of acceleration from solids [Allen et al., 2004; Fuchs et al., 2005]. Antici et al. [2007] report on some of the first experiments performed to explore the regime of ion acceleration using ultra-thin targets

interacting with an ultra-high temporal contrast 320 fs duration laser pulse. Proton beams accelerated to a maximum energy of ~7.3 MeV from targets as thin as 30 nm thick and for a 10^{18} W.cm^{-2} laser intensity were observed. Neely et al. have also reported [2006] results using similar targets in ultra-high contrast conditions. Here, using a much lower on-target laser intensity and a longer pulse (10^{18} W.cm^{-2} and 320 fs) than Neely et al. (10^{19} W.cm^{-2} and 33 fs), ~2 times higher proton energies were obtained. It was also shown that this acceleration regime produces nearly a tenfold increase of proton maximum energy as compared to the standard regime using thicker targets at the same laser intensity. PIC simulations in close agreement with the measurements suggest that enhanced target electron heating as compared to thicker targets results in the observed proton energy increase. In the simulations much higher proton energy increase is predicted for similar target thickness and somewhat higher laser intensities (3-6 10^{19} W.cm^{-2}).

As in the rear-surface acceleration process with thick targets, ion acceleration in the relativistic transparency regime involving ultrathin targets is observed in simulations to be lead by the fast electrons accelerated by the laser from the front side into the target, except that a higher number of electrons are heated to higher temperatures as the result of the interaction of the laser pulse with the whole volume of the ultra-thin target. Emerging from the target, these electrons form a dense electron plasma sheath at the vacuum interface that accelerates surface ions [Hatchett et al., 2000], mostly hydrogen-rich contaminants [Gitomer et al., 1986].

In the standard regime of thick targets, the proton energy increase for decreasing target thickness is due to a reduced spreading of the fast electrons within the target as discussed in Section 2.1. For the relativistic transparency regime, an optimum target thickness is predicted to be reached when the laser absorption in the target equals the laser transmission [d'Humières et al., 2005], in practice it is in the range of tens to hundreds of nm. At the peak intensity levels (> 10^{18} W/cm^2) required to accelerate ions to large energies, the pedestal pre-leading the main pulse, or ASE (laser amplified spontaneous emission), is generally high enough to ablate such thickness of target material. More importantly, it also induces rear-surface target heating prior to the arrival of the main pulse for thin targets (still thicker than the ablated thickness), reducing the ion energy. This has limited the minimum target thickness to few microns in typical high-energy ion acceleration experiments. This is why laser pulses need to be contrast enhanced in order to explore this relativistic transparency regime. The ultrahigh contrast can be achieved using several methods like self-induced plasma shuttering from solids [Doumy et al., 2004], or frequency doubling of the laser wavelength. Both induce similar reduction in laser energy but the latter has the further disadvantage of decreasing the $I\lambda^2$ factor.

A maximum proton energy of ~7.3 MeV was recorded during these experiments using two plasma mirrors to be able to use thinner targets. The targets were 30 nm thick SiN planar membranes uncoated or coated with a variable thickness of Al. Without plasma mirrors, the laser interaction with ultra-thin targets yielded no result (probably because the target material was evaporated before the main pulse) and the laser interaction with 5 μm thick

targets also yielded a maximum energy below the detection threshold, i.e. <0.9 MeV. At similar laser intensities, the proton energy increase going from thick target with a standard contrast to ultra-thin targets with ultra-high contrast was thus higher than a factor 8. Equivalently, to reach similar proton energies in the standard regime of thicker target having cold rear-surfaces, much higher laser intensities are needed, e.g. 2 10^{19} W.cm^{-2} for 25 µm thick targets [Fuchs et al., 2006]. Laser to proton energy conversion, calculated by considering protons from 1.8 MeV (resp. 4 MeV) to the maximum energy is 4 % (resp. 1.1 %) for 30 nm thick target, 3.7 % (resp. 0.9 %) for 80 nm thick target, and 2 % (resp. 0.4 %) for 100 nm thick target. Note that when the same maximum proton energy is reached in the regime of thicker targets at much higher laser intensity, the laser to proton energy conversion is much lower, i.e. ~0.1 % for protons from 4 MeV to the maximum energy. The angular distribution of the proton beams is also observed to be irregular, on the contrary to proton beams accelerated at similar maximum energies from thick metal targets which display a very smooth profile. This could be due to the fact that the focal spot in presence of two plasma mirrors is not optimized.

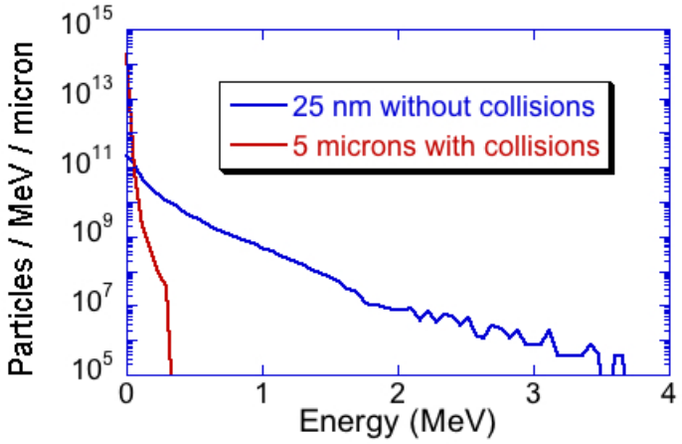


Figure 3. Electron spectrum obtained from the 2D PIC simulations for a 25 nm thick target and a 5 microns target, a 350 fs pulse duration, and a 1.38×10^{18} W/cm^2 laser intensity.

Simulations performed using the 2D PIC code PICLS [Sentoku and Kemp, 2008] of the interaction of a prepulse-free laser pulse with a thin dense target allow to get an insight on the interaction conditions. The incident laser pulse has a 1 µm wavelength, a 350 fs pulse duration, an intensity of 1.38×10^{18} W/cm^2, and a transverse spot size on target of 6 µm FWHM. The temporal and spatial (transverse) profiles are Gaussian and the laser electric field is in the simulation plane. The laser interacts at normal incidence with the 25 nm thick, 100 n_c density target, initially fully ionized, that consists of a layer of Al surrounded by two layers of hydrogen.

The maximum proton energy is 7.33 MeV, as observed 2.8 ps after the beginning of the simulation, in close agreement with the observation. Performing a simulation with the same parameters but adding the treatment of collisions yields a very close maximum proton energy of 7.28 MeV, as can be expected since in such conditions where the target is heated efficiently, the jxB absorption significantly dominates collisional absorption. In both simulations, we observe negligible transmission. The consistency between experiment and

simulations support the fact that in the experiment the main laser pulse could interact with a solid density target.

To understand the specific mechanism of proton energy increase obtained using ultrathin targets, an additional simulation using a thicker, i.e. 5 μm thick, target still at 100 n_c, with collisions was performed. These simulations show a higher heating for ultrathin targets compared to the thicker target. We have to note that the laser absorption is comparable for the two targets (~23 %). It is the partition of the absorbed laser energy into the cold and hot electron populations that differs significantly between the two target thicknesses, as shown in Figure 3. In the thicker target, a high number of electrons remain cold and the maximum electron energy is low. In the ultrathin target, the hot electrons spread around the whole target and the maximum electron momentum is high. This is due to the target heating induced by the hot electrons, which are not damped by the cold background as in the thicker target, leading to a density lowering of the target, and an enhanced absorption in hot electrons for subsequent parts of the laser pulse.

Interaction with ultrathin targets leads to a very efficient electron heating, and high proton energies. Going towards longer pulse durations also favors absorption in hot electrons in ultra-thin targets since the trailing part of the pulse can take advantage of the target heating induced by the leading part and of the increased absorption. This explains the increased proton energy observed in these experiments using 320 fs duration pulses as compared to experiments performed with 30 fs duration pulses [Neely et al., 2006], although the intensity used here is ten times lower.

The experiments and simulations presented here show the potential of laser-acceleration of protons from ultra thin targets using ultra-high contrast pulses. In the present experiment, exploring of this regime has been limited to the threshold of the relativistic regime. Both the low efficiency of the consecutive plasma mirrors and the low final focal spot quality are strong limitations. In future studies, this could be improved by adjusting the fluence on the mirrors. It has been indeed demonstrated that 50 % efficiency with good focusing quality could be obtained from two successive mirrors [Wittmann et al., 2006]. This would allow achieving intensities above 10^{19} W/cm^2, thus working with an optimum configuration for the same target thicknesses. In this case, as shown in [Antici et al., 2007], 2D simulations show that very high proton energies (> 100 MeV) should be obtained. Around 120 MeV protons and GeV Carbon ions were recently measured in this regime at the Los Alamos National Laboratory [Jung, 2012]., breaking the existing world records, and plasma mirrors are now routinely used in laser ion acceleration experiments with ultrathin targets.

3. Laser ion acceleration using low density targets

In this Section experimental and theoretical studies on laser ion acceleration with low density targets are presented. This regime offers a promising alternative to the accelerating regimes described in Section 2. The basics of this regime are described and some recent experimental and theoretical results are also discussed.

As discussed in sections 1 and 2, intense research is being conducted on sources of laser-accelerated ions and their applications, e.g. radiography and production of Warm Dense Matter (see review articles [M. Borghesi et al., 2006; J. Fuchs et al., 2009]). This is motivated by the exceptional properties that have been demonstrated for proton beams accelerated from planar targets (see Section 2), such as high brightness, high spectral cut-off, high directionality and laminarity, and short duration (~ps at the source). In most experiments, solid density targets, typically gold or aluminum, are used and the most energetic ions are accelerated from the rear side by a strong electrostatic field created by fast electrons (through the so-called TNSA mechanism). This section presents a different setup aiming at studying the possibility of enhancing the efficiency and ease of laser acceleration of protons and ions compared to what has been achieved up to now using standard TNSA.

Indeed, it is not only important for applications of such ion beams that their parameters (maximum energy and total number) are enhanced, but also that they are easily usable. Regarding the second point, there are currently some issues/limitations linked with using solid targets: 1) targets need to be aligned precisely for each shot, 2) laser temporal contrast needs to be controlled, 3) debris are produced, 4) repetition rate is limited. These limitations would all be greatly alleviated if one could use gas jets as the laser interaction medium. Following preliminary theoretical [Esirkepov et al., 1999; Yamagiwa et al., 1999; Sentoku et al., 2000] and experimental [Krushelnick et al., 1999; Sarkisov et al., 1999] studies on ion laser acceleration using underdense targets, ion acceleration from low density targets was recently the subject of growing attention [Willingale et al., 2006; Yogo et al., 2008; Antici et al., 2009; Willingale et al., 2009]. However, the efficiency of the process was not shown to be high. For example in [Willingale et al., 2006], the maximum energy of the ions produced this way was only half of the one that could be obtained using solid targets.

There are several interpretations about the (best) production of the proton beam in gaseous conditions. One hypothesis is that the protons are produced by electrostatic acceleration at the target–vacuum boundary like in TNSA, although this was subject of debate [Willingale et al., 2007]. For example, acceleration of energetic ions observed by Willingale et al. had been explained in terms of strong inductive electric fields due to magnetic fields variations on a steep density gradient [Bulanov et al., 2007]. Through simulations, it has been found that shock acceleration could be used in such low-density medium to accelerate ions not only very efficiently, but also with a comparable number as TNSA [d'Humières et al., 2010a]. The basic idea behind it is that lower density targets can improve the absorption of the laser energy, hence both the laser-to-ion conversion and the ion energies can be enhanced. However, to reach such optimum working point, precise interaction conditions need to be met. With present-day laser parameters, it requires rather thin gas jets (of the order of 100 microns), which are not readily available. So, in parallel of working to produce such gas jet, it was proposed to work on demonstrating such optimum of ion acceleration exploiting shock acceleration in lower-than-solid density targets [d'Humières et al., 2010b]. For this, it is possible to use, as a substitute for optimized gas jet, targets that have been exploded by a secondary laser prior to the arrival of the main beam. The goal is not only to

demonstrate the existence of optimized ion acceleration beyond TNSA, but also to shed light about these processes.

Test experiments have recently been performed at LULI (France) demonstrating the effectiveness of ion acceleration in the regime which had been explored through simulation. However the laser intensity and energy during that experiment were somewhat limited (~J) [Gauthier et al., 2012]. As PIC simulations (see below) show that this acceleration process is more efficient with higher intensities and longer pulse durations, doing experiments on that topic using higher energy lasers would be very beneficial as it would allow to effectively test the increased efficiency of shock acceleration in the domain where it is seen by simulations to be best: with long pulses and high laser energy. This, coupled to progresses on gas jets, would strongly enhance the practicality and possibilities for ion probing or warm dense matter generation on future high-power and high rep-rate laser facilities.

As found out by 1D and 2D Particle-In-Cell simulations performed with the PICLS code with respect to previous experiments using exploded foils having low-density [Antici et al., 2009], the ion acceleration processes in these plasmas depend strongly on the characteristics of the density gradient. For sharp and small density gradients, the most energetic protons are accelerated at the back surface, similarly as in TNSA. The acceleration mechanism is then similar to the one observed with solid foils. For intermediate density gradients, the most energetic protons are accelerated by a collisionless shock mechanism in the decreasing density ramp at the target exit. A two-step acceleration process takes place: first, ions are accelerated in volume by electric fields generated by hot electrons, second, the ion energy is boosted in a strong electrostatic shock, as shown in [E. d'Humières et al., 2010a]. If the density profile becomes too long, the shock cannot be triggered and ions are accelerated by normal expansion in the density gradient which is a low efficiency mechanism [Grismayer and Mora, 2006].

Collisionless shocks have already been studied in decreasing density gradients for spherical plasmas [Peano et al., 2007] and for plasmas located at the back of a solid foil irradiated by a laser [Tikhonchuk et al., 2005]. In [d'Humières et al., 2010b], and [E. d'Humières et al., 2011a; E. d'Humières et al., 2011b], the shock regime and the two step process were studied in detail. The first step, the launch of a fast ion wave, requires a hot electron population and a descending density profile and occurs in a zone of high amplitude magnetic fields. This first step has already been described theoretically by Grismayer and Mora [2006] but since the authors used a Lagragian code, they could not go beyond this first step. The second step, the development of a strong electrostatic shock which boosts the energy of the ions, happens when the ion bunch resulting from the first step enters a low density plasma region where the magnetic field has strongly decreased. The first 3D simulation of this regime were recently performed [d'Humières et al., 2011a] and confirmed the 2D simulation results. Using 1D PIC simulations, it was also confirmed that this regime does not require a high magnetic field to launch a strong collisionless shock. A Vlasov-Poisson code is presently used to study in more details the processes described and to obtain scaling laws of the maximum proton energy and accelerated

proton numbers with laser and target parameters [d'Humières et al., 2011b]. The number of accelerated protons is high, similar to what is observed with TNSA, and could be higher as it is possible to accelerate ions in a thicker region of plasma even if the density is low in this region, whereas TNSA is limited to a small region inside the back of a target where the strong electrostatic field can be felt. As exemplified by Figure 4, 2D PIC simulations show that to reach this high efficiency regime, a high laser energy is needed for low density plasmas with a high thickness by density product. The fact that it is difficult nowadays to produce these types of plasmas except from exploded foils naturally gives an advantage to large-scale facilities with several tens of Joules in the main pulse and several tens of Joules in the exploding pulse.

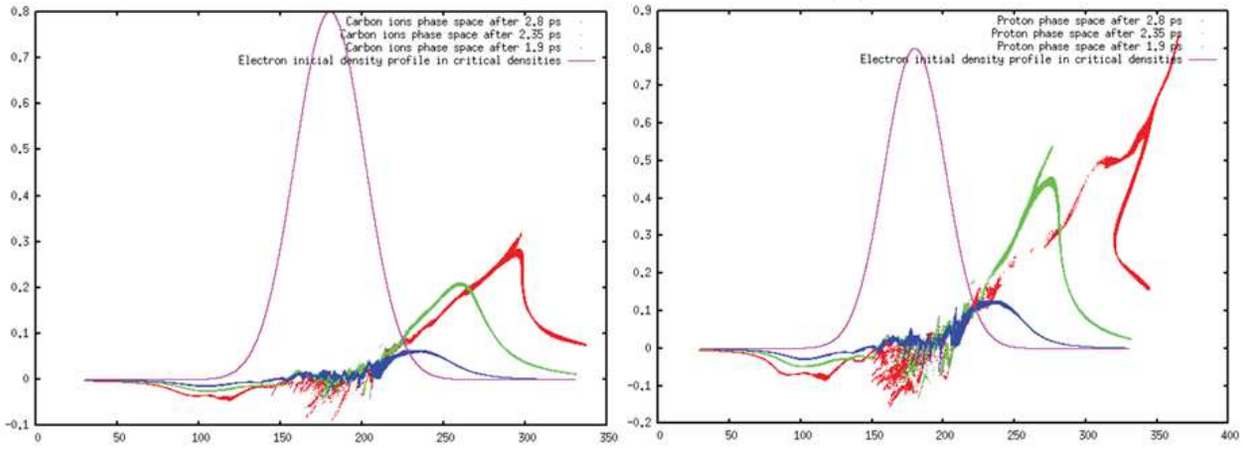


Figure 4. (right) Proton phase space at three different times (1.9 ps after the beginning of the simulation for the blue dots, 2.35 ps for the green dots and 2.8 ps for the red dots) and initial electron density profile (purple line, units of critical density). The laser is injected from the left. The target is composed of Carbon ions, protons and electrons and its FWHM is 50 microns. Laser intensity is $5x10^{20}$ W/cm^2, pulse duration is 700 fs FWHM and the focal spot width is 6 microns. Maximum proton energy at t=2.8 ps is 281 MeV. It reaches 296 MeV after 3 ps. The development of the ion wave is clearly visible at t=1.9 ps and the shock is launched just before t=2.35 ps and has fully developed at t=2.8 ps. (left) Carbon ions phase space at three different times (1.9 ps after the beginning of the simulation for the blue dots, 2.35 ps for the green dots and 2.8 ps for the red dots) and initial electron density profile (purple line, units of critical density). The Carbon ion wave is clearly visible at t= 1.9 ps and 2.35 ps and the shock on Carbon ions starts to develop just before t=2.8 ps. This is later than for the shock on protons. This is normal as the Carbon ion wave takes more time to develop than the proton wave. Maximum Carbon ion energy is already 496 MeV at t= 2.8 ps. It reaches 889 MeV after 4 ps. In both cases, the x-axis is in microns and the y-axis for the phase spaces represents beta*gamma where beta is the ion velocity divided by the velocity of light and gamma is the proton Lorentz factor.

As illustrated in Figure 4, preliminary simulations using the TITAN (LLNL) laser parameters were performed. These show the extremely interesting potential of this regime since in the simulations 296 MeV protons and ~900 MeV C ions are accelerated. Other simulations using TITAN parameters but exploring different target thickness of plasmas (still peaking at 0.8 n_c) have been performed. For all cases, the production of energetic particles is linked to strong electrostatic shocks. More simulations and experiments are needed to fully grasp the potential of this regime and to optimize it.

4. Optimization of laser ion acceleration with various types of targets

In this Section, several innovative studies on the optimization of the characteristics of laser accelerated ion beams are presented. New targets were recently tested to change the interaction conditions, the electron sheath characteristics or the ion distribution. These studies have allowed to find new ways to increase the maximum ion energy, as well as new ways to decrease the beam divergence and energy spread. Several of these targets or setups are described here. Other targets have recently been investigated to improve the coupling of the laser energy with the target electrons but are not described in this Section. Klimo et al. [2011] have for instance tested nano-structured targets to enhance the coupling between the laser and energetic electrons.

4.1. Laser ion acceleration using micro-cones

Studies of the interaction of energetic laser pulses with micro-cones using PIC simulations have been performed in collaboration with experimentalists from Los Alamos National Laboratory and the University of Nevada, Reno. The importance of the geometry of the cone on the increase of the laser energy absorption and of the hot electron temperature was highlighted. It was also shown that these targets are very sensitive to the laser alignment and contrast. Coupling these cones with flat micro-disks, it is possible to strongly increase the maximum proton energy [Flippo et al., 2008] while also increasing the obtained ion beam divergence [Renard Le Galloudec et al., 2010].

The basics of laser ion acceleration with micro-cones are detailed in this Section as well as recent theoretical, experimental and numerical results. The world record in maximum laser accelerated protons energy was broken in 2009 using these types of targets [Gaillard et al., 2011]. A proton beam with energies as high as 69 MeV was obtained using 80 J of laser energy whereas the previous record had remained at 58 MeV [Snavely et al., 2000] for almost 10 years and needed 500 J.

Cone targets are of interest for their potential to increase the hot electron temperature and population density [Sentoku et al., 2003a; Kodama et al., 2004], which are the main contributors to the efficacy of the TNSA mechanism. Sentoku *et al*. [2003a] showed that sharp tip cones can effectively increase the number of electrons available for laser heating while guiding the laser light along the cone wall surface toward the cone apex. This action tremendously increases the interaction area of the laser, producing more electrons and concentrating the laser field at the cone neck near the flat-top surface. UNR physicists in combination with the nano-fabrication group, NanoLabz, were able to design a relatively inexpensive process for mass producing a new type of cone target (Figure 5.a). A process with obvious advantages over the hand-assembled ICF targets to date. Early results have shown these cones can produce excellent ion beams when properly aligned.

Pioneer experiments performed on the Titan laser (LANL) showed that the flat-top cone produces more protons at higher energies than the flat foil, in this case 13 times more above 10 MeV [Flippo et al., 2008]. The total energy present in the beam from the Au flat-foil is

measured to be 0.4% of the incident laser energy. When this is done for the flat-top cone target it is measured to be 1.9% of the incident laser energy. This represents a nearly 5 fold increase in the conversion efficiency over the Au flat foil targets and a 3.4 fold increase in the total amount of protons, with nearly 13 times the number above 10 MeV. The proton beam observed from the cone target contains two orders of magnitude more protons than previous experiments at similar intensities [Maksimchuk et al., 2004] and is more than two orders of magnitude more efficient (laser energy conversion to protons) than previously published work for a similar laser intensity [Fuchs et al., 2005] and energy [Fuchs et al., 2005; Borghesi et al., 2006]. The beam also has a 3 to 5 times higher maximum proton energy than previously reported for a similar intensity from flat foils [Fuchs et al., 2006; Robson et al., 2007], at least 1.5 times that of the Trident flat foil, and potentially more than 2 times that of the flat foil as simulations indicate.

The cone targets have been modelled with the particle in cell code PICLS. One simulation was performed exactly matching the experiment at a laser wavelength of 1 μm with an intensity of 10^{19} W/cm^2, a pulse duration of 600 fs and a focal spot of 12 μm. The cone inner neck diameter was 10 μm, and the flat-top thickness was 13 μm with a diameter of 90 μm. Maximum proton energy reached almost 40 MeV (Figure 5.b). Several other simulations where performed as part of a parameter study at a laser wavelength of 1 μm and an intensity of 10^{19} W/cm^2, but with a pulse duration of 350 fs and a FWHM spot of 6 μm to keep the calculation time to a minimum. The various simulations are summarized in [Flippo et al., 2008]. The cone parameters have been varied to highlight the main advantages and drawbacks of the flat-top micro-cones and to understand the driving factors behind the observed enhancement. They reveal that the cone leads to significantly improved laser energy absorption and conversion to hot electrons when well aligned, resulting in higher hot electron temperatures and densities. These increases due to the flat-top cones, which are a function of the cone neck-diameter and opening angle [Nakatsutsumi et al., 2007], provide a potential advantage for laser-ion acceleration as these are the main parameters governing the TNSA accelerated ions [Wilks et al., 2001].

At these laser parameters (1 μm laser wavelength, 350 fs pulse, 6 μm spot size, and 10^{19} W/cm^2 intensity), the flat-foils have been observed experimentally to produce ~3-5 MeV [Fuchs et al., 2006a] for a 20 μm thick target. The simulated flat-foil, which is 10 μm thick, results in a proton maximum energy of 8.6 MeV. This higher energy is consistent with the fact that the thinner simulated target follows the experimental trend of increasing proton energy for a thinner target at the same laser parameters [Mackinnon et al., 2002; Fuchs et al., 2006a]. The smooth cone with a 10 μm inner diameter neck and 10 μm thick walls (for a total neck outer diameter of 30 μm) has the highest performance, yielding a maximum proton energy of ~26 MeV, with a 90 μm top and a top-to-neck ratio of 3. Comparatively, a cone with a 20 μm inner diameter (total of 40 μm) with a top to neck ratio of 2.25 yields 10 MeV, a 62% decrease. Here, when the neck size is increased by a factor of two the electron temperature, the maximum electron energy, and the proton maximum energy are all decreased by about the same factor. Combining information from [Flippo et al., 2008], one can deduce that the neck diameter has a stronger influence on the maximum proton energy

and electron temperature than the flat-top diameter. However, it is evident that both dimensions play a role; and thus, their ratio is still a good figure of merit.

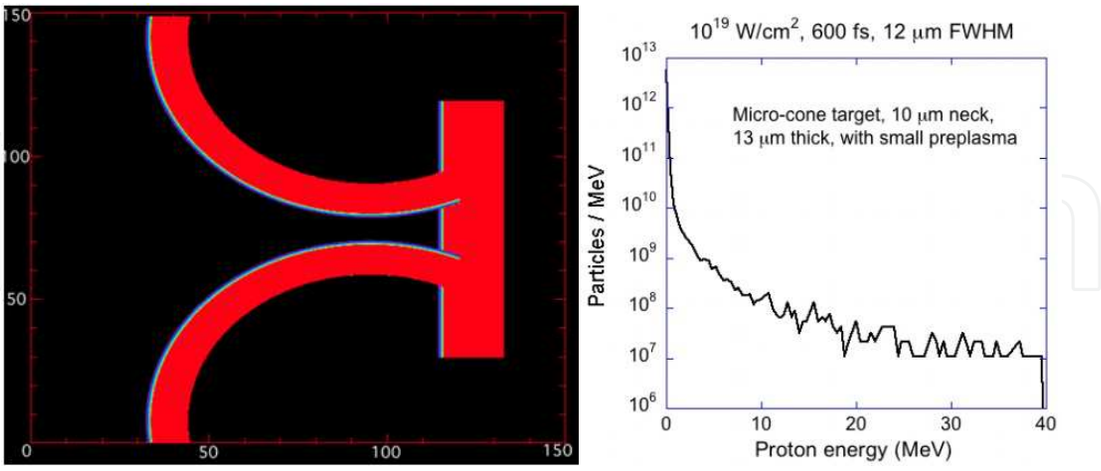


Figure 5. (a) Illustration of the shape of the flat-top cone geometry. Axis are in microns (from 0 to 150 microns). (b) Simulated proton energy spectrum.

One can conclude that for the TNSA mechanism to work efficiently, a smooth surface on which a dense, hot sheath can form is essential. A sharp-tip cone would not be suited for this application, and results have not shown promise for such cones to be used as proton beam generators. One also needs to transport the many hot electrons efficiently to the flat-top surface from wherever the hot electrons are generated. This last point can be described as the hot electron population transport characteristic of the cones. The transverse pointing accuracy can have a major effect on this transport. The farther the laser is focused away from the cone axis, the longer and more complex the path is to the flat-top for the hot electrons. On the way, these electrons can be scattered and lost to other areas of the cone or slowed down by the transfer of energy to the ions present on the rear surface of the cone side-walls. The overall hot electron population and temperature is shown to be only slightly affected by the increase in transverse offset distance; whereas the maximum proton energy is largely perturbed, decreasing by a factor of eight. This is caused by the electrons inability to be efficiently transported to the flat-top, and instead spread out over the relatively large surface area of the cone's side-walls [Flippo et al., 2008].

Another issue affecting the hot electron population, temperature, and transport is the preplasma filling in the inner cone neck. As long as the laser is able to propagate through the preplasma without significant filamentation, a higher density preplasma can enhance the coupling to the hot electrons, which can effectively lead to an increase in the maximum ion energy. However, if the laser is strongly affected by a denser preplasma and is instead reflected, dispersed, or entirely absorbed far from the flat-top, then any hot electrons generated must travel a longer distance to arrive at the flat-top. As in the case of the transverse pointing accuracy, the hot electrons will be scattered or decreased in energy traversing the longer path, or completely lost to forming the cone side-wall sheath, never making it to the flat-top. As the density of the plasma inside the cone neck increases the

distance between the interaction zone and the flat-top increases. When the level of preplasma density inside the cone neck is increased from $0.001n_c$ to $2n_c$ on the laser axis (increasing exponentially to $10n_c$ at the cone wall interface), the laser is not able to reach the flat-top. Although the laser absorption has been increased to 83.2%, the maximum proton energy is decreased to 18.8 MeV due to the effect of the longer electron transport distance to the flat-top. Nevertheless, the simulated maximum proton energy is still more than 2 times higher than that from the simulated flat-foil target, an attribute of the enhanced laser absorption and hot electron temperature.

To gauge the effect of the longitudinal focusing, two simulations were performed such that the laser was focused both on the flat-top as well as 80 microns prior to the flat-top (the Rayleigh length is 100 microns in these conditions). The laser absorption, hot electron temperature and maximum proton energy are only slightly changed. This is consistent with the observation that the curved cone geometry dilutes the longitudinal pointing accuracy differences as seen in [Sentoku et al., 2003a]. The main reason for the increase in the maximum proton energy comes from the cone guiding the laser light allowing more energy transfer to electrons as well as a neck diameter being of the right dimensions so as to form a thick, underdense, preplasma for efficient hot-electron generation and a short undisturbed transport to the flat-top.

It has therefore been shown that laser-ion acceleration with flat-top cones is a novel and an efficient method to obtain high quality energetic ion beams. PIC simulations have also shown that the maximum energy of the accelerated ions is proportional to the hot electron temperature and density, and is inversely proportional to the hot electron transport distance. The cone wall smoothness is an important factor to optimize the maximum ion energy, while the longitudinal pointing accuracy has only a small influence on the final proton energy. As long as the laser axis is aligned with the cone axis and as long as the preplasma is not sufficiently dense to affect laser propagation toward the cone tip, the maximum ion energy depends only on the hot electron population characteristics, which is influenced by the cone geometry and not necessarily by the flat-top size. If the preplasma level is high or if the laser is not well aligned, even the higher electron temperatures and densities will not be sufficient to overcome the effect of the elongated electron transport path and associated scattering to the cone side-walls. The long transport results in proton spray emission from the cone side-walls and poor ion beam quality and efficiency.

New target concepts along with new ideas to achieve ignition of fusion targets with laser and particle beams are presently of high interest and have a wide range of applications in the field of high energy density physics. Studies of the cone target along with other shapes have paved the way to enable a better understanding of the cone physics allowing to develop the cone target presented in the rest of this section along with its relevance for an array of applications [Renard-Le Galloudec et al., 2010].

For such a target to give its full potential, because of the physics occurring in a cone, some criteria need to be met (the same as the ones above). The cone target needs to be precisely aligned. The laser enters the cone and starts hitting the faces when its diameter is about 3 to 4

times the inside tip size [Sentoku et al., 2004; Nakamura et al., 2007; Renard-Le Galloudec et al., 2008]. Under low preplasma conditions [Sentoku et al., 2004; Renard-Le Galloudec et al., 2008], so as to not destroy the conical shape the laser interacts with, the cone microfocuses the laser light into the tip [Sentoku et al., 2004]. At the same time, the laser interacts with the faces of the cone, creates electrons and guides them along the faces to the tip where the electron beam gets out [Renard-Le Galloudec et al., 2009]. This increases dramatically the electron density in the tip, enables a higher conversion efficiency of laser light into very energetic or hot electrons [Sentoku et al., 2004; Nakamura et al., 2007; Nakamura et al., 2004; Nakatsutsumi et al, 2007], and thus enhances both electrons and protons [Chen et al., 2005]. Note here that the cone, not the laser, defines the beam diameter [Renard-Le Galloudec et al., 2008]. A smaller cone angle produces more energetic electrons compared to a more open cone [Nakamura et al., 2007; Chen et al., 2005]. In addition, cones show an increased absorption of the laser light compared to flat targets [Nakamura et al., 2007], which makes them more efficient. More complex cone-based geometries have also been studied [Flippo et al., 2008] and also show an increased efficiency compared to flat targets.

In [Renard-Le Galloudec et al., 2010], both the inside and outside tip of the cone are slightly curved. Shaping the back of flat targets has been demonstrated to focus protons beams [Wilks et al., 2001; Ruhl et al., 2001; Roth et al., 2002; Patel et al., 2003; Snavely et al., 2007], it is however the first time that this concept is adapted to a cone geometry in order to use cones as an essential element of the particle beam production and reap the benefits of the increased efficiency of its shape. It does more than a standard flat or curved target. It adds three essential aspects. The first aspect is that making use of the cone faces by allowing the laser to spread on them greatly reduces the amount of preplasma filling the cone, thus enabling an efficient use of the cone shape. It also uses the faces to create the electrons and guide them to the tip. Several articles have showed the imprint of the laser pattern on flat targets into the particle beam [Fuchs et al., 2003]. As the laser bounces several times on the faces on its way to the tip, its imprint disappears. It creates, at the tip, a laser imprint free area of high energy density, enabling more uniform beams. Also, if best focus is positioned toward the entrance of the cone, then all of the laser light available gets in regardless of the fnumber of the focusing optic compared to the cone angle. The second aspect is the fact that the cone, then, not the laser, defines the particle beam [Renard-Le Galloudec et al., 2008]. The laser is clearly not directly driving the characteristics of the beam produced. The third aspect is the ability to control the divergence of the output beam. The tip of the cone is slightly curved in this case. This results in a modification of the divergence of the output particle beam by effectively modifying the accelerating sheath shape, and can be tuned by adjusting the amount of curvature. This efficiently produces a beam with extremely relevant characteristics to various applications. With high-energy high-repetition rate lasers as well as targets that are on the verge of cost effective mass production, cost effective compact applications can be readily envisioned.

Because the new target shape proposed in [Renard-Le Galloudec et al., 2010] has not been fabricated yet, the 2D Particle-In-Cell (PIC) code PICLS was used to run simulations and

assess the electromagnetic fields structures and proton beam characteristics in comparison with flat targets. Several intensities were run to span the range available to short pulse lasers. The inner and outer tip diameters are respectively 10 and 30 μm. They are both curved. The target itself is 10μm thick. The incident laser pulse (1 μm, 40 fs, 21 μm FWHM transverse spot size at 3×10^{18} W/cm^2) has a Gaussian temporal and transverse spatial profile. The laser interacts with the target at normal incidence, with its polarization in the simulation plane. The initial target density is $40n_c$ and remains higher than the relativistic critical density a_0n_c, where a_0 is the normalized laser amplitude and n_c is the critical density ($n_c = 1.1 \times 10^{21}/\lambda\ (\mu m)^2 cm^{-3}$, λ is the laser wavelength). The plasma is composed of Al ions, protons and electrons.

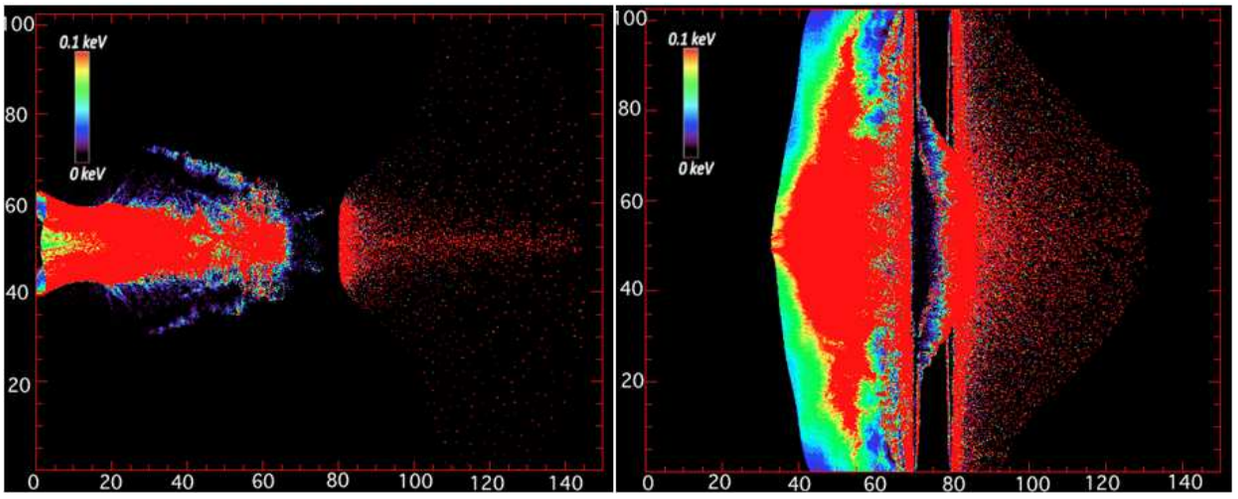


Figure 6. Proton energy density for the cone target at 3.10^{20}W/cm^2 (6.a) and for the flat target for the same laser intensity (6.b). The pulse is injected to the left. Axis are in microns from 0 to 150 for the x-axis and 0 to 102 for the y-axis.

Figure 6.a represents the 2D proton energy density for a 10μm thick curved-tip cone in a high intensity case at 3.10^{20}W/cm^2. Figure 6.b represents the same 2D proton energy density for a 10μm flat target at the same intensity. We clearly see that the protons are a lot more confined in the cone than in the flat target where they tend to diffuse laterally. The particles emitted from the cone are much more collinear to the laser axis compared to the flat target where they expand perpendicularly to the sheath.

In both cases the average divergence is small, especially for the high-energy protons. While the cone target does not seem to do better for these, it does control the divergence much better than the flat target over a wider range of energies. The curvature also allows to focus the most energetic protons in a specific location, and thus to deposit through the ions a higher energy in a smaller volume than in the case of a flat target, which is of special interest to isochoric heating.

The results in [Renard Le Galloudec et al., 2010] confirm that the cone is a much more efficient structure over a range of intensities (from 3×10^{18} W/cm^2 to 3×10^{20} W/cm^2). As the

intensity increases, the maximum proton energy increases in general regardless of the target but the cone target clearly shows higher maximum proton energy than the flat target for all intensities. That difference increases with intensity. Especially evident at 3.10^{20}W/cm^2, both electrons (fig. 7.b) and protons [Renard Le Galloudec et al., 2010] are accelerated to higher energies in a higher number for the cone target. Enhanced laser interaction results in much higher maximum proton energies at high intensities (from 54.4 MeV to 98.7 MeV). Laser absorption is greatly increased in cone targets. In the high intensity case, laser intensity reaches a maximum of 2.4 10^{21} W/cm^2 in the tip of the cone (6.10^{20} W/cm^2 for the flat target), highlighting the microfocusing effect of the cone. In the low intensity case, the large preplasma present in both cases tends to give similar laser parameters evolutions, similar electric fields and a moderate increase of maximum proton energy (see Figure 7.a). In the high intensity case, the laser intensity and the longitudinal electric field reach significantly larger values in the cone leading to an important increase in maximum proton energy.

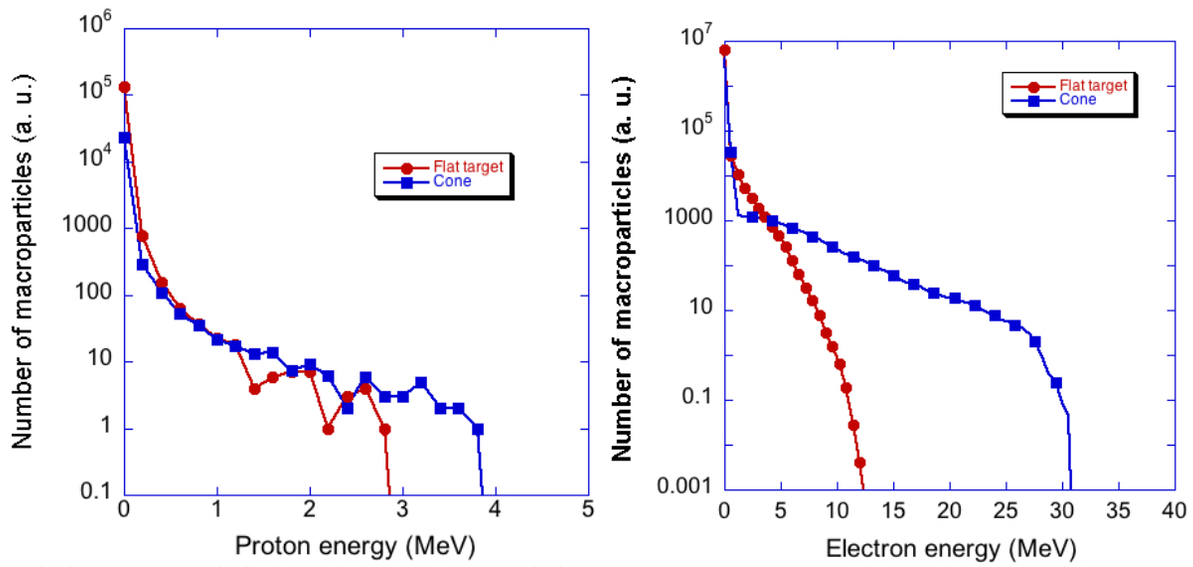


Figure 7. Proton energy spectrum (7.a) for both cone and flat target at 1.98ps for the low intensity case, and electron energy spectrum (7.b) for both cone and flat target at 924fs in the high intensity case.

It is therefore shown that this new conical target shape has the potential to produce proton beam of a higher maximum energy, a higher intensity and a lower divergence. Because of the appropriate use of the cone structure itself, by using the faces leading to the tip, it is also shown that the target itself defines the proton beams characteristics, nor the laser imprint or the focal spot size have an impact on these characteristics. The contrast of the laser can also be mitigated and finally the fnumber of the focusing optic is superseded by that of the cone target itself. All these parameters increase the potential for various groups to join in the research endeavour and pursue exciting new applications.

4.2. Laser ion acceleration using reduced-mass targets

The coupling between high intensity laser pulses with solid foils having a limited transverse extension (~ few tens of μm) has been studied by diagnosing electrons and protons produced during this interaction [Buffechoux et al. 2010]. It was observed that by reducing the area of the target surfaces, it is possible to reflect electrons near the edges of the target during and just after the laser irradiation. This transverse refluxing, which does not occur with usual large planar targets, can maintain a hotter, denser and more homogeneous accelerating electron sheath. As a consequence, when this transverse refluxing takes place during the ion acceleration duration, the maximum ion energy and the conversion of laser energy in the energy of high energy ions are strongly increased. The ion beam divergence is also reduced thanks to the more homogeneous electron sheath. These results will be detailed in this Section. Since, new experiments performed in 2011 using such targets allowed to obtain proton energies of around 80 MeV [Schollmeier et al., 2011].

The dynamics of MeV electrons generated in solids by ultra-intense lasers plays a crucial role in many applications such as electron-driven fast ignition [Tabak et al., 2006] or the production of secondary sources, e.g. X-rays [Quéré et al., 2006], positrons [Chen et al., 2009] or ions [Fuchs et al., 2009], all with important scientific or societal perspectives.

Understanding the hot electrons dynamics requires considering several aspects of their transport through the target. This Section reports an investigation of the influence of the target lateral dimensions on the dynamics of hot electrons and associated energetic proton production [Buffechoux et al., 2010]. It was the first to identify the important role played by the lateral electron recirculation in small targets. As observed in the simulations discussed here, electrons that are injected into the target center are seen to spread along the target surface with a velocity v^t_{hot} ~0.7c and reflected at the target edges. They therefore transit from the center to the edges and back in a time $\tau_t=D_s/v^t_{hot}$ where D_s is the target transverse diameter. When τ_t is of the order of the laser pulse duration τ_L, the hot electrons, refluxing from the edges, are confined during or shortly after τ_L. This leads to a time-averaged denser, hotter and more homogeneous electron population. This has been observed through the use of a combination of hot electrons and accelerated proton diagnostics.

The effective (time-averaged) hot electron temperature (T_{hot}) as a function of the target surface area was analyzed [Buffechoux et al., 2010]. It was observed that both N_{hot} and T_{hot} increase for targets having surface areas $<3\text{-}4\times10^4$ μm², corresponding to target transverse diameters D_s<170-200 μm. For larger targets, both T_{hot} and N_{hot} remain, on the contrary, constant. With regards to T_{hot}, the data are consistent with simulations of sharp-interface plasmas irradiated at 45° with S polarization [Lefebvre et al., 1997]. With regards to N_{hot}, the data are consistent with measurements of hot electrons density (n_{hot}) and sheath surface [Antici et al., 2008a] which, combined, yield comparable number of electrons contained in the sheath. All these results are consistent with previous complementary measurements that showed an increase of bulk target heating when reducing the target surface area [Nakatsutsumi et al., 2008; Perez et al., 2010].

It was also observed that the hot electron sheath becomes more uniform when the target surface area is reduced. This result is obtained by analyzing the angular proton beam profile as recorded on the RCF film. It is shown that the beam is more collimated when the target surface area is reduced. This suggests a flatter electron sheath along the target rear side for smaller targets, which is consistent with the picture of geometrically confined electrons. The measurement of the thermal emission from the target rear side further confirms this. As a result of the observed increase of N_{hot} and T_{hot} within the electron sheath, when reducing the target surface area, a clear improvement of the proton beam characteristics was observed (maximum proton energy and laser-to-proton conversion efficiency).

Two-dimensional (2D) particle-in-cell (PIC) simulations of laser target interactions were performed to help identify that lateral refluxing of the hot electrons is the key process leading to hotter, denser and more homogeneous electron sheaths when reducing the target surface area. The mechanism of refluxing, as observed in the simulations, is as follows: because of their high velocity, electrons trajectories can be considered as ballistic. As electrons enter the target with an angle close to the laser incident angle (45°), their average transverse (with respect to the target normal) velocity in the target is $v^t_{hot} \approx c \times \cos(45) = 0.7c$. After several reflections off the sheath fields on the front and back surfaces with that same angle, the electrons will have travelled transversely to the edge of the target to be again reflected back (note that here there is no distinction between electrons turning around the target and electrons reflected back).

Since the electric field accelerating the ions is proportional to $(n_{hot}T_{hot})^{1/2}$ [Fuchs et al., 2009; Mora, 2003], proton acceleration is expected to be enhanced for the small foil compared to the medium foil, and indeed the simulation results agree well with the variation of the experimental proton cutoff energies. The enhancement in ion acceleration can take place only if the electrons can come back to the target center within the ion acceleration time τ_{acc}. From this, an experimental proton acceleration time can be deduced $\tau_{acc} \approx 800\text{-}950$ fs. This is consistent with theoretical estimates. Also in good agreement with the experimental result, simulation results show that refluxing produces in the simulations a more uniform sheath in small targets. The constrained lateral dimension forces the hot electrons to recirculate in the small foil, thus homogenizing the sheath.

Reducing the surface area of solid targets therefore leads to an increase in the effective hot electron number and mean energy due to the lateral electron recirculation. In particular, this effect enhances the properties of laser-accelerated ions, in terms of energy, flux and collimation, as necessary for progress towards applications. Use of this simple mechanism is of interest for future experiments at higher intensity laser facilities, but will impose high temporal contrast laser pulses to avoid preplasma leakage to the target rear-surface. In addition, progress in target fabrication will offer targets that are not only of reduced lateral size, but also thinner as it is now found favorable for ion acceleration (see Section 2.3).

4.3. Focalization of laser accelerated ions using curved targets

The dynamics of the focusing of laser accelerated ions using curved solid targets has been intensively studied in the last years [Patel et al., 2004; Kar et al., 2011; Chen et al., 2012]. The ability to tightly focus, i.e. over tens of microns, dense (> 10^{10} particles), short (with duration ~ps) bunches of positively charged particles is far beyond the possibility of present particle accelerators. The increase of the particle density of these beams would significantly improve the efficiency and prospects of a number of important applications. High energy density proton beams would allow, for example, igniting pre-assembled Inertial Confinement Fusion (ICF) targets, also known as proton Fast Ignition (PFI) [M. Roth et al., 2001], or enable ultrafast heating, above keV, of dense materials to explore their properties [Mancic et al., 2010; Pelka et al., 2010; Carrié et al., 2011]. High energy density positron beams would allow enhancing the rate of antimatter creation in the laboratory [Andresen et al., 2007], opening up investigations of many fundamental laws of nature.

These positively charged beams, broadband or monoenergetic, can nowadays be produced with a high particle number and over a short duration using ultra-intense, short pulse lasers interacting with solids targets [Wilks et al., 2001; Chen et al., 2010] as described in Section 2. When using flat targets as sources, the ion beam is divergent, 0-25 degrees depending on proton energy [Fuchs et al., 2003; Roth et al., 2005; Toncian et al., 2006], since the expanding sheath field front on the target rear-side is Gaussian in shape [Romagnani et al, 2005; Antici et al., 2008]. Such divergence can however be compensated by curving the back surface of the target, so that the accelerated proton beam will converge [Patel et al., 2003; Kar et al., 2011; Offermann et al., 2011]. This points to the necessity of understanding and optimizing the dynamics of the focusing sheath in order to achieve tight focusing, as necessary for the above-mentioned applications.

A study of the ion beam focusing dynamics through temporally and spatially resolved measurements, with picosecond and micrometer resolution, of the shape of the sheath field from a curved target, irradiated by a high-intensity short pulse laser has recently been performed [Chen et al., 2012]. Experiments performed at LULI show that the major part of the energy carried by ions converge at the center of cylindrical targets in a spot having a diameter of 30 microns, which can be beneficial for applications requiring high ion energy densities. The location of the focus is a function of proton energy, although most of the protons focus at the geometric target center. It was also shown experimentally and using 2D PIC simulations that the exact location of laser illumination on the curved target does not adversely affect the ability to focus the sheath-accelerated ion beam, although it modifies the directionality of the ion beam. Despite these advantages, an important filamentation was observed during the focusing, which limits the energy deposition precision in the ion converging zone. This effect is important for the use of such a setup in order to obtain high ion energy densities. It is the case in the fast ignition concept with ions which requires to have a high ion concentration zone with a diameter of 10 to 20 microns. Simulations have shown that at higher laser intensities, closer to the ones expected to be used for ion fast ignition, ion focusing was improved.

4.4. Acceleration of quasi-mono-energetic ions beams using the TNSA mechanism

For many potential applications of laser accelerated ions, controlling the characteristics of the produced ion beam is essential. Several techniques have recently been tested to obtain quasi-mono-energetic ion beams using the TNSA mechanism. Using either a secondary laser to control the thickness of the layer of ions accelerated to high energies [Hegelish et al., 2004], or small plastic dots to reduce the transverse extension of the accelerated proton bunch [Schoewer et al., 2004], these techniques try to constrain the acceleration zone to avoid acceleration gradients and therefore limit the ion energy spread. Another possibility to control the energy spread as well as the beam divergence has recently been developed. This technique consists in using a tuneable plasma microlens that allows focusing the ion beam and selecting specific energies. The control of the characteristics of proton beams using a solid cylinder irradiated by a secondary laser has therefore been studied [Toncian et al., 2006; d'Humières et al., 2007] using simulations and experiments performed at LULI (France). This Section explains these various techniques and discusses their limits (Figure 8).

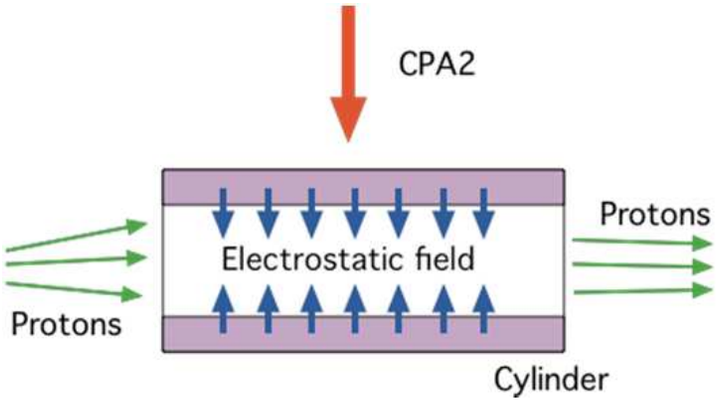


Figure 8. Schematic of the micro-lens setup focalizing a proton beam propagating on its axis. The proton beam is accelerated from a planar metallic foil by a first laser pulse. The proton beam is focalized using the hollow cylinder irradiated on the side by the laser pulse CPA2.

The focalization is effective only for a range of energies: as the cylinder is located at a certain distance from the source, and as the source has a large spectrum, protons with different energies have different times of flight and therefore reach the cylinder at different times. If the high energy protons cross the cylinder before it is irradiated by the secondary laser generating the focalizing fields, they do not undergo any focalizing effect (it is the case of the picture on the left in Figure 9). Protons with a slightly lower energy, synchronized with the focalizing fields will undergo the maximum effect. This is illustrated by the simulations performed in Figure 9.

The focalization symmetry is also observed in PIC simulations [d'Humières et al., 2006] and comes from the fact that fast electrons, even if they are produced in one region of the cylinder wall, propagate faster on the whole diameter than it takes them time to expand in

vacuum towards the interior of the cylinder. Therefore, when the plasma expansion into vacuum phase, at the origin of the focalizing radial electric fields, starts, the radial distribution of these fields is symmetric.

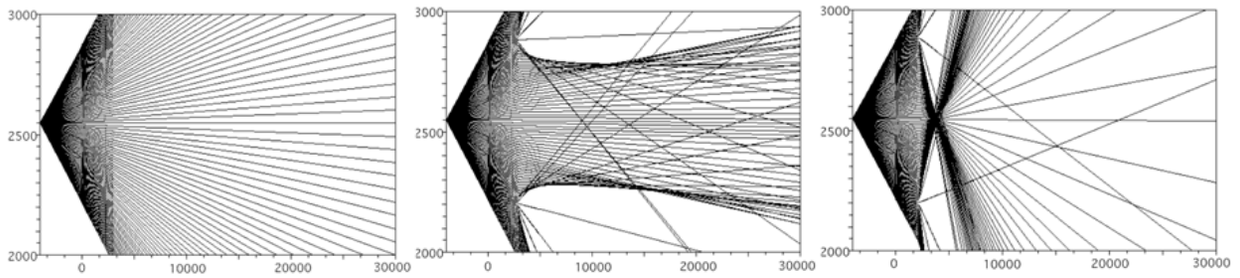


Figure 9. Trajectories of 100 protons at (a) 7.6 MeV; they exit the cylinder (located at x=0) before it is irradiated and their divergence is not affected. The two axis are in microns but at different scales. (b) Protons at 6.25 MeV; they are close to the exit of the cylinder when it is irradiated, sustain small fields and are therefore well collimated. (c) Protons at 4.9 MeV; they are at the middle of the cylinder when it is irradiated, they therefore sustain fields much stronger than the ones on b). They are therefore focalized at a short distance (5 mm) from the cylinder and then strongly diverge.

It appears that this micro-lens (its diameter is typically of the order of a mm, as well as its length) has the advantage, compared to curved targets, to allow a focalization which is not limited to distances of a few mm. It also allows to move away the source from the focalization region, which can be interesting for instance in the perspective of fast ignition using proton beams: increasing the distance between the two would allow to avoid damaging the source during the implosion of the main target. The focalization distance can indeed be tuned simply by varying the intensity of the beam generating the focalizing fields.

The fact that the focalization distance is variable as a function of energy can be exploited to select in energy in a controllable manner part of the spectrum, which is initially large. It is then enough to position a small opening at a calculated distance from the cylinder. A small number of high energy protons (crossing the cylinder before the focalization) will go through the opening. The protons with a focalizing distance corresponding to the distance between the opening and the cylinder will all be transmitted leading to a peak in the spectrum while the protons with lower energies will be focalized before the opening and will therefore reach it unfocused, and a small number of them will cross the opening. The position and the width of the peak can be easily adjusted by tuning the intensity and the delay between the pulse triggering the micro-lens and the primary pulse generating the source, as well as by tuning the distance between the micro-lens and the source.

The use of the micro-lens is not limited to protons. Therefore, the micro-lens presents the advantage, in comparison with previous solutions, of being able to achieve focalizing as well as energy selection in a single step. Moreover the process is simple: the pulse triggering the micro-lens requires just 10% of the main pulse, the micro-lens is cheap (it is just a section of what is used for medical syringes), it does not require any particular target engineering, and finally it is easy to change the desired parameters (focalization distance, size of the focalization point, energy of the protons to be focalized, peak to be selected in energy, width

of this peak) by adjusting the laser parameters (intensity, delay between the two pulses) and the cylinder-source distance.

This development, achieving compact collimation of energetic ions, is therefore an extremely important step towards applications of laser accelerated ion sources. These advantages compared to existing (conventional) setups can be summarized as:

- Compactness: mm instead of dm.
- Capability to focus beams of several A instead of several mA; the last two points are the results of the fact that it is a plasma setup, therefore able to sustain much higher electric fields than conventional setups.
- Selective collimation in a few ps.
- Capability to focus in a few mm, cm or m multi-MeV beams in place of a minimum of a few meters for conventional setups or not more than mm for curved targets.

5. Laser ion acceleration limits in the ultra high intensity and ultra high laser energy regimes

With the recent rapid progresses in high power laser technologies, new laser systems are under construction and will allow to explore the ultra high intensity regime (Apollon in France and then ELI in Europe) and the ultra high energy regime (OmegaEP at Rochester, PETAL in France, ARC at LLNL and FIREX in Japan). This section presents the limits of the laser ion acceleration mechanisms described in the previous sections in these extreme regimes. These studies aim at obtaining a better understanding of how the predictions given by the existing laser ion acceleration models will be affected in these regimes and to estimate more realistically their potential.

5.1. Laser ion acceleration in the ultra high intensity (UHI) regime: Effects of radiation losses

Several PIC codes have recently been modified to take into account radiation losses by charged particles [Sokolov et al., 2009a; Tamburini et al., 2010; Capdessus et al., 2012] These models were then applied to the study of laser ion acceleration in the ultra high intensity regime (> 10^{22} W/cm^2) [Naumova et al., 2009; Tamburini et al., 2010; Capdessus et al., 2012; d'Humières et al., 2012] when radiation losses become important and can not be neglected anymore. This section discusses these results and shows how, in this regime, radiation losses strongly depend on the target density, thickness and on the laser pulse polarization. Even if radiation losses always lead to electron cooling, their effect on the ion distribution depends on the interaction conditions. For thin and moderate density foils, radiation losses can even enhance laser ion acceleration while decreasing electron heating [Capdessus et al., 2012]. These results have been confirmed using 2D PIC simulations [d'Humières et al., 2012].

A new generation of laser systems such as planned in the Extreme Light Infrastructure (ELI) project [http://www.extreme-light-infrastructure.eu/] will produce laser intensities as high

as 10^{24}W/cm^2. New physical processes are expected under these conditions such as emission of high energy photons, the radiation reaction force acting on electrons, electron-positron pair production, acceleration of ions to relativistic energies, etc. [Bulanov, 2009]. One of the important applications of ultra intense laser pulses is acceleration of charged particles to extremely high energies. Recent numerical simulations and theoretical analysis show that at laser intensities exceeding 10^{22} W/cm^2 the ions can be accelerated to relativistic energies under the laser radiation pressure. While the radiation reaction force has been applied to the motion of a single particle for a long time, it has only recently been considered in plasma physics. First kinetic simulations of laser plasma interaction with a particle-in-cell (PIC) code accounting for the radiation force were reported in Refs. [Naumova et al., 2009; Schlegel et al., 2009; Tamburini et al., 2010, Chen et al., 2011]. They demonstrated the role that the radiation reaction plays in the radiation pressure acceleration by high intensity laser pulses.

The effect of radiation losses on the process of ion acceleration by ultra intense laser pulse has also been studied in 1D in [Capdessus et al., 2012]. This effect becomes important for laser intensities exceeding 10^{22} W/cm^2, where the radiation friction force slows down electrons and affects the ion dynamics through the self-consistent electrostatic field. The effect of radiation losses depends strongly on the target density and thickness and also on the laser polarization. It is less important in the case of strongly overdense targets and for a circular polarization, where the relative density n_e/n_c is larger than the laser amplitude, a_L. This is explained by clear spatial separation of the particles and fields. On the contrary, the radiation losses are important in the induced transparency regime where $n_e/n_c < a_L$. Although radiation losses are always leading to cooling of electrons, their effect on the ion distribution depends on the target thickness. In the case of thin targets, where the areal density is small, radiation losses may improve ion acceleration. On the contrary, in the piston regime, radiation losses lead to a reduction of the piston velocity and less efficient ion acceleration. These simulation results were limited to 1D simulations. However, the particle momentum has three components and arbitrary angles of electron propagation with respect to the laser wave are accounted for. No qualitative changes in 2D or 3D simulations are therefore expected. Recent results published in [Tamburini et al., 2012] confirm that statement. They demonstrated that results obtained for lower dimensionality remain valid qualitatively, although the maximum energy of ions in 3D is found to be higher than in corresponding simulations in 1D and 2D. The self-generated magnetic fields are also expected to be responsible for stronger radiation emission.

2D simulations were performed in [d'Humières et al., 2012]. The goal was to study how laser ion acceleration using thin overdense targets evolves in the ultra high intensity regime (> 10^{22} W/cm^2) and to assess the importance of radiation losses in this regime. The radiation losses model used is based on the so-called Sokolov model [Sokolov et al., 2009a]. In a first set of simulations, the wavelength of the incident pulse is 0.8 μm, its pulse duration is 21 fs and its irradiance is 1.6×10^{22} W/cm^2. The FWHM of the focal spot is 5 μm. The p-polarized Gaussian pulse interacts with the target in normal incidence. The plasma is composed of protons and electrons with a constant 400 n_c density. The plasma slab thickness was varied from 0.2 to 0.8 μm. Figure 10.a shows the simulated proton spectra with and without

radiation losses for the 0.5 μm case. In this range of thicknesses, radiation losses have a measurable effect on ion acceleration but this effect remains small. In a second set of simulations, the wavelength of the incident pulse is 0.8 μm, its pulse duration is 48 fs and its irradiance is 1.5×10^{23} W/cm^2. The FWHM of the focal spot is 5 μm. The circularly-polarized trapezoidal pulse interacts with the target in normal incidence. The plasma is composed of deuterons and electrons with a constant 10 n_c density. The plasma slab thickness was varied from 0.4 to 5 μm. Figure 10.b shows the simulated electron spectra with and without radiation losses for the 5 μm case. For such a high intensity the radiation losses effects become important and the energetic electron population is strongly affected. Very high ion energy are nevertheless obtained (a maximum energy of 1.8 GeV for Deuterons in the 5 μm case) [d'Humières et al., 2012].

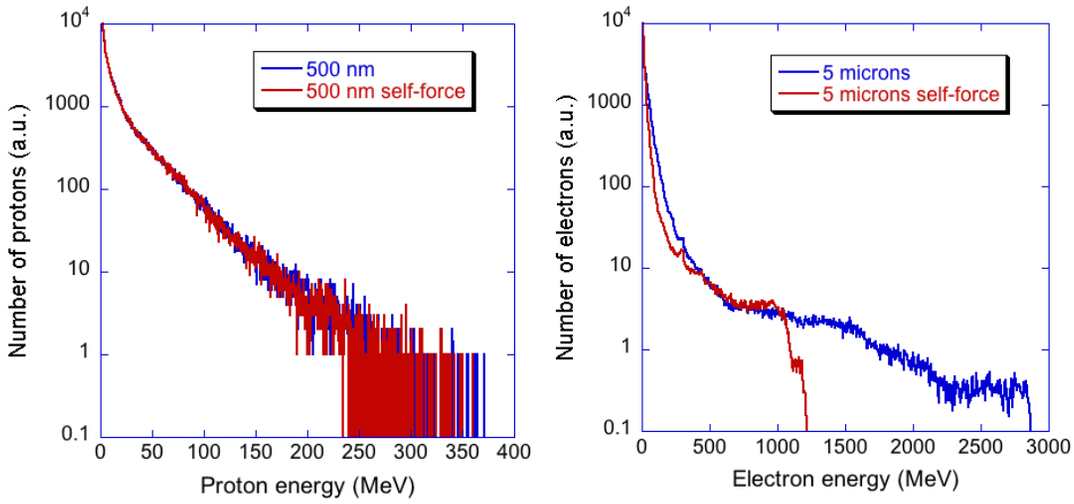


Figure 10. (a) Proton spectra for the 1.6×10^{22} W/cm^2 pulse interacting on a 500 nm high density foil. (b) Electron spectra for the 1.5×10^{23} W/cm^2 pulse interacting on a 5 μm overdense foil. Blue curve: without radiation losses. Red curve: with radiation losses.

The interaction of a high intensity short pulse with overdense targets is now actively studied in the UHI regimes to estimate ion acceleration possibilities on future laser facilities. This study is performed using Particle-In-Cell codes in which charged particles energy losses through radiation have been implemented. In the ultra high intensity regime, radiation losses will start affecting laser ion acceleration using thin overdense targets for intensities higher than 10^{22} W/cm^2, but maximum proton energies of a few hundreds MeV can still be reached.

5.2. Laser ion acceleration in the ultra high energy (UHE) regime

The interaction of a ultra high energy (up to 3.5 kJ) and high intensity laser with various types of targets has recently been modelled using PIC simulations to prepare laser ion acceleration experiments on high energy installations [d'Humières et al., 2012]. Laser ion acceleration in the ultra high energy regime (> 1 kJ) has also recently been studied experimentally [Flippo et al., 2010]. This section presents a study of this regime to analyze

the changes brought by such high laser energies on the main accelerating mechanisms presented in the previous sections. Energies of more than 100 MeV can be obtained in a robust manner using solid foils with thicknesses of a few tens of μm. These beams could then be used to radiograph the implosion of a DT target when coupling PETAL with the LMJ for instance, or for other experiments (isochoric heating, laboratory astrophysics…).

A new era of plasma science started with the first experiments on the National Ignition Facility (NIF) at the Lawrence Livermore National Laboratory (LLNL) in the USA. The Laser MégaJoule (LMJ) under construction near Bordeaux in France is following the trail opened by the NIF with its planned 160 laser beams for more than 1 MJ to reach ignition of a deuterium - tritium target using the indirect drive method. Besides the physics of ICF (plasma physics, shock / fast ignition), NIF & LMJ will be essential for basic science, exploring fields such as plasma astrophysics (e.g. study of shocks to simulate violent events in the Universe such as supernovæ, accretion disks), planetary physics (highly compressed and warm matter), stellar interiors with large coupling between radiation field and matter & nuclear physics. A petawatt short pulse laser will be added to the ns pulse beams of the LMJ. This is the PETAL system (PETawatt Aquitaine Laser) [Blanchot et al., 2008], under construction on the LMJ site near Bordeaux (France) and funded by the Région Aquitaine. The ultimate goal is to reach 7 PW (3.5 kJ with 0.5 ps pulses). For the beginning of operation, the PETAL energy will be at the 1 kJ level, corresponding to an intensity on target of ~ 10^{20} W/cm^2.

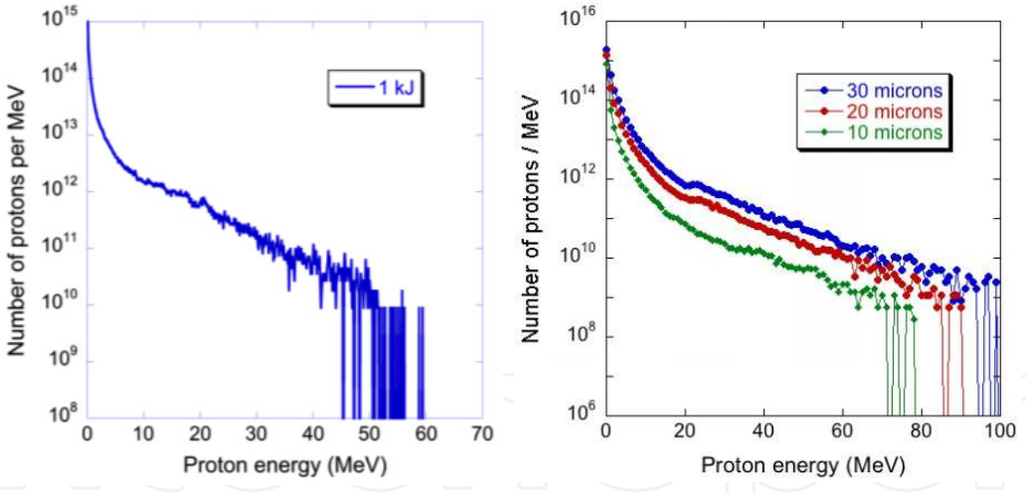


Figure 11. (a) Computed proton energy spectrum emitted from the PETAL target with 1kJ energy. (b) Variation of the proton energy spectra for three laser FWHM: 10 μm (green line), 20 μm (red line) and 30 μm (blue line) with 1.75 kJ at 2ω.

In the experiments proposed for LMJ - PETAL, the petawatt laser may be focused on a secondary target, where a short (~ 20 ps length) bunch of particles (electrons, protons, ions) is produced and may be used to probe the plasma generated by the ns LMJ pulses. The energetic ions are produced using the TNSA mechanism detailed in Section 2. First calculations were performed using the 2D particle-in-cell code PICLS to compute the energy spectra and angular divergences of the protons produced with PETAL (Fig. 11.a) for 1 kJ of

energy in the PETAL beam and for 3.5 kJ. Protons with a maximum energy higher than 100 MeV are measured in the 3.5 kJ case. Within these conditions, these calculations can be considered as majoring the intensities and electron energy spectra end-points. After the accurate characterization of the particle emission from the PETAL target, the diagnostics will be used for plasma experiments, which, for example, requires proton radiography to determine the magnetic field or the electric field structure at the plasma scale or to measure the density of the LMJ plasmas.

Multi-kJ Petawatt-class laser systems therefore open new and exciting opportunities for laser ion acceleration. The interaction of a high intensity short pulse with underdense, near-critical and overdense targets has been studied using 2D Particle-In-Cell simulations in these regimes [d'Humières et al., 2012]. The goal was to study laser ion acceleration in the ultra high energy regime (> 1 kJ). 2D Particle-In-Cell simulations were performed to study the interaction of the expected PETAL laser pulse with a thin target in the transparency regime [Dong et al., 2003; d'Humières et al., 2005]. The wavelength of the incident pulse is 1 μm, its pulse duration is 500 fs and its irradiance is 10^{21} W/cm^2. The FWHM of the focal spot is 30 μm. The p-polarized Gaussian pulse interacts with the target in normal incidence. The plasma is composed of protons and electrons with a constant 400 n_c density. The plasma slab thickness was varied from 0.2 to 1 μm.

The maximum proton energy measured in the simulation depends on target thickness and reaches several hundreds of MeV at 1ω. The results in [d'Humières et al., 2012] indicate that the most energetic protons come from the rear surface of the target. It will not be straightforward to accelerate protons with such thin targets without controlling the laser contrast. A plasma mirror or doubling the frequency could improve this contrast. With a 250 nm foil and at 2ω (limiting the total energy to 1.75 kJ), the maximum proton energy is lowered to 160 MeV and 3.1×10^{10} protons/MeV at 100 MeV are expected. Figure 11.b shows the variation of the proton energy spectra for three laser FWHM: 10 μm (green line), 20 μm (red line) and 30 μm (blue line). As expected, the number of protons at high energies increase with the laser FWHM. The maximum proton energy also increases but at a slower rate. A simulation using a 10 microns CH target at solid density with a preplasma and similar laser parameters predicts a maximum proton energy of around 110 MeV.

Another promising way to accelerate ions to high energies is to use underdense or near-critical density targets (see Section 3). The interaction of a laser pulse with a near-critical density target and an underdense target was simulated using the above laser parameters in 2D. In both cases the plasma is composed of protons and electrons. For the first case, the target density is constant and its thickness is 100 μm. For the underdense case, the target density profile is a cosine square with a full-width at half maximum of 100 μm and a maximum density of 0.4 n_c. A high laser absorption of 75.9% is measured in the 2 n_c case and 18.9% is measured in the 0.4 n_c case as the laser propagates through the plasma leaving a large channel behind. The generated hot electron population produces strong electrostatic fields at the back of the target.

Figure 12 shows the proton spectra in both cases (a) and the proton phase space at the middle of the simulation box on the laser propagation axis 0.99 ps after the beginning of the simulation (b). For both cases the most energetic protons come from a region close to the back surface of the target. Wave breaking is clearly visible in the underdense case as expected from previous theoretical studies. The maximum proton energy in the near-critical case is more than 400 MeV, which is comparable with the solid density target simulation, and 7×10^9 protons/MeV at 200 MeV are expected. It reaches a little more than 200 MeV in the underdense case with 2×10^{10} protons/MeV at 100 MeV.

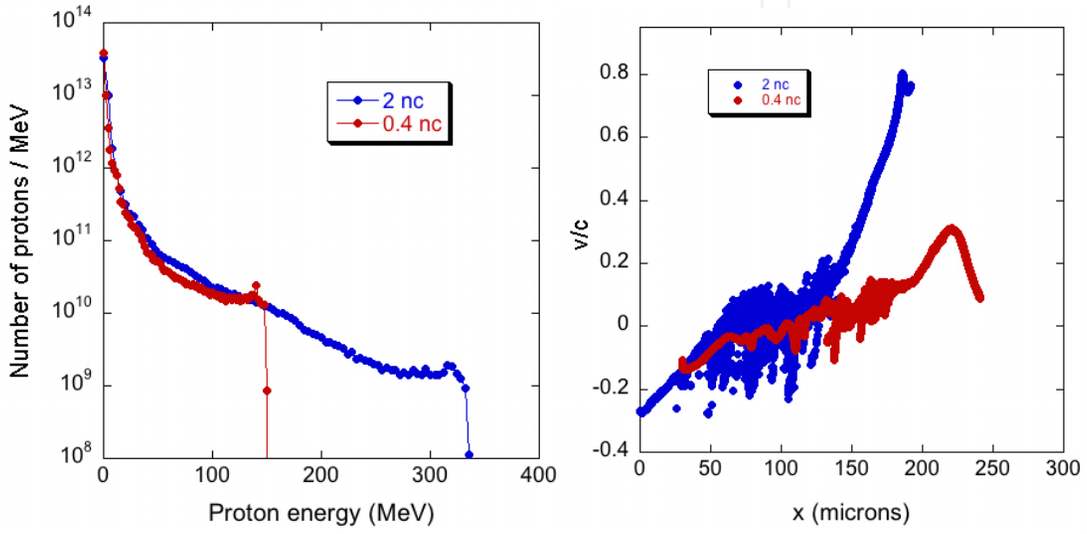


Figure 12. (a) Proton spectra for the 2 n_c case (blue line) and for the 0.4 n_c case (red line). (b) Proton phase space at the middle of the simulation box on the laser propagation axis 0.99 ps after the beginning of the simulation.

Interaction conditions are not optimized. In this low density regime it is possible to find an optimum thickness and a key parameter controlling the acceleration process is the product of the density and the thickness. This optimum thickness also depends on laser parameters. The interaction of a PETAL laser pulse with a low density target could therefore lead to even higher maximum proton energies than solid targets. The near-critical target could be achieved experimentally using a foam, an aerogel or a cryogenic target, the underdense target using a gas jet or a foil exploded by a nanosecond pulse (see Section 3).

The interaction of a high intensity short pulse with underdense, near-critical and overdense targets has therefore been studied with 2D PIC simulations in the UHE regime to estimate ion acceleration possibilities on future laser facilities. In the ultra high energy regime, proton beams with maximum energies of several hundreds of MeV and a high number of high energy protons could be accelerated using thin solid foils or underdense and near-critical targets.

6. Applications of laser ion acceleration

As described in the previous sections, laser ion acceleration has already been applied to diagnose electromagnetic fields in plasmas and to produce warm dense matter. Other important applications are envisioned in laboratory astrophysics, as injectors for conventional accelerators or for the production of radioisotopes and hadrontherapy. Several of these promising applications of laser accelerated ions are presented in this section. This list, which is not exhaustive, aims at illustrating the important potential of compact high intensity ion accelerators.

6.1. Laser accelerated ions as a diagnostic of hot electron transport in dense targets

The possibility to control the shape of MA electron currents in solids by high intensity laser pulses has been studied using different target materials [Sentoku et al., 2011]. This Section details how these effects can be diagnosed using laser accelerated ion beams as the accelerating electron sheath is affected by the transport of the hot electron beam. These results are beneficial to applications like the production of secondary sources and the ion fast ignition concept for inertial confinement fusion.

Ultra-high currents (MA) of suprathermal (MeV) electrons, that are driven through solids using relativistic laser pulses (with intensity $I > 10^{18}$ W/cm^2), lie at the heart of numerous applications, either present-day like the generation of ultra-short secondary sources of particle and radiation (ions [Malka, 2008], X-rays [Mancic et al., 2010b], positrons [Chen et al., 2010], or neutrons [Disdier et al., 1999]), or potential like fast ignition of inertial confinement targets [Tabak et al., 1994] or laser-driven hadrontherapy [Bulanov et al., 2002a; Fourkal et al., 2002; Malka et al., 2004]. Having the possibility to spatially shape these currents is crucial in order to optimize the efficiency of each process. Sentoku et al. [2011] showed by combining experiments and modelling, how dynamical shaping of the currents can be achieved in various conductor materials. By tuning the target ionization dynamics that depends both on the target material properties and on the input electron beam characteristics, it is possible to control the growth of resistive magnetic fields that feedback on the current transport. As a result, collimating, hollowing or filamenting the electron beam can all be obtained and observed on the laser accelerated ions characteristics.

For all these applications, metals are preferable as target materials as they can provide enough cold electron return current to neutralize the forward laser-generated current and allow its propagation at current levels (MA) exceeding the Alfven critical current [Alfven, 1939]. At solid density, such targets are little prone to the Weibel relativistic electromagnetic two-stream instability [Weibel, 1959; Sentoku et al., 2003b] that is collisionally damped [Sentoku and Kemp, 2008]. Instead, resistive magnetic fields have been suggested to play more of a role [Kar et al., 2009; Robinson et al., 2007; Storm et al., 2009; Solodov et al., 2010]. These fields, that could collimate or focus the otherwise divergent electron beams [Debayle et al, 2010; Perez et al., 2010b], are driven by the Ohmic fields with the resistivity

dynamically changing during target heating due to the hot electrons flow. The fields evolve according to Faraday's law. Weighting the role of magnetic fields has been relying up to now on hybrid simulations. These however present significant limitations due to their inability to self-consistently model the laser-generated hot electron source evolving at the dynamically ionizing interface. This has thus limited so far our understanding of the magnetic fields influence and impacted the possibility to adequately and quantitatively plan future progress, e.g. in designing fast ignition targets [A.A. Solodov et al., 2009] for present large-scale international programs [M. Schirber et al., 2005]. It is now possible to use Particle-In-Cell codes treating relativistic collisions and ionization processes to solve this issue.

Modulations of the sheath potential near the target surface will be imprinted in the protons angular distributions as they are detaching from the rear surface during the acceleration [H. Ruhl et al., 2004]. In [Sentoku et al., 2011], the 10 μm thick Au target exhibits a single peak distribution with the tightest profile, consistent with the experimental observation. The 15 μm thick Cu target on the other hand has a twin peak distribution, also consistent with the doughnut pattern of the experimental measure. Finally, the 40 μm thick Al target has a lower potential, since it is the thickest target, with a wider and modulated distribution, again consistent with the experiments. The trends observed in the experiment when increasing the target thickness or reducing the laser energy, i.e. a disappearance of the modulation in Cu or Al, are also observed in simulations performed with PICLS using collisions and ionization. For a 40 μm Cu target, strong ionization ($Z>15$) proceeds in a distance $x \sim 15$ μm, which is consistent with the heated region seen in the electron energy density map. Thus, strong resistive magnetic fields only grow in this region before breaking into weak filaments, ~ 5 MG, that cannot modulate strongly MeV electrons. As a result, the electrons spray out and form a smooth sheath potential at the target rear surface. Similar simulation results from reduced laser energy cases were also obtained.

The technique of manipulating the target resistivity developed here allows, even using a monolithic material, to control MA current flows in solids, e.g. excite the pinching, hollowing or filamenting of the currents. For this, the target thickness should be equal to or a bit thinner than the propagation distance of ionization waves during the laser pulse duration. Beyond the demonstration in [Sentoku et al., 2011], an important practical point is that keeping the same laser energy but changing the laser intensity (by e.g. defocusing the laser or increasing the pulse length), one can engineer transporting the same electron charge through different spatial form, e.g. pinched or hollowed out. Diagnosed using laser accelerated protons, it could help get higher maximum proton energies and smoother proton spatial distributions.

6.2. Magnetic lens for laser accelerated ions

High resolution proton deflectometry has been applied to measure magnetic fields in dense plasmas in order to quantitatively compare with simulations of the evolution of the magnetic field produced by intense electron currents generated by high intensity short laser

pulses [Albertazzi et al., 2012]. Indeed, as seen in Section 6.1, such magnetic fields have the potential to limit the divergence of fast electron beams, a crucial factor in the context of secondary sources production or for achieving fast ignition of fusion targets. The capacity to measure these fields allows to have a better understanding of the implied physical mechanisms and to optimize them. In Section 6.1, these fields were diagnosed directly by ions leaving the target. In this section, two targets are used: one to accelerate protons and a second one irradiated by a secondary laser and radiographed by the proton beam coming from the first target.

Preliminary studies [Sentoku et al., 2003b] have shown that one of the main mechanisms to achieve collimation of of an energetic electron beam could rely on self-generated magnetic fields. These fields grow in the solid since the fast electron beam is not neutralized everywhere by the cold return current. The magnetic field arises from the resistive electric field $\mathbf{E} = \eta\mathbf{j}$ which depends on the resistivity η and on the current $\mathbf{j}$. Taking into account Maxwell-Faraday equation, two terms for the temporal derivative of the variation of the magnetic field can be obtained [Sentoku et al., 2011]. One term is a current term and the other one is a resistive term. This last term depends on the collision time, atomic number of the target, temperature and time since the resistivity will evolve in time. In order to study the influence of the self-generated magnetic fields on the transport of fast electrons, the self-generated magnetic fields were measured using face-on proton radiography and the influence of target material was also studied [Albertazzi et al., 2012]. Using a plasma mirror and thin targets, it was possible to probe self-generated magnetic fields in dense target. The experiment gives the dynamics of this self-generated magnetic field over a very large time: ~100 ps. The temporal dependence of the magnetic field patterns shows a field inversion which appears at different times for different materials. 2D PIC simulations including ionization and collisions performed with the code PICLS and coupled to test particles simulations using the fields obtained with the PIC simulations have allowed to reproduce some important features of the experiments and thus to better understand the physical mechanisms at play. This setup can also be used to constitute a magnetic lens to improve the characteristics of laser accelerated ions (divergence and energy spread).

6.3. Collision of laser accelerated plasmas to study collisionless shocks for astrophysics

Ion beam instabilities play an essential role in the formation of collisionless shocks in laser-plasma interaction or in astrophysics. Weakly relativistic shocks are considered as potential sources of high energy cosmic rays. Experiments performed in the laboratory would allow to have a better understanding of the microphysics involved in this process. As demonstrated in the previous sections, laser systems delivering short high intensity laser pulses can accelerate ions to high energies. Low energy electrons neutralize these ion beams. It is therefore possible to produce counter-propagating beams to study the collision of fast plasmas and the formation of collisionless shocks (Figure 13) [Kato et al., 2008; Davis et al., 2010; Davis et al., 2012].

Collisionless shocks are an ubiquitous phenomena in the Universe. Weakly relativistic shocks are created in supernova explosions. It is believed that relativistic shocks are responsible for strong electron heating, magnetic field generation and subsequent emission of hard X and gamma rays in Gamma Ray Bursts (GRB). Collisionless shocks are considered to be a source of energy redistribution in Nature and high energy cosmic rays. However, a detailed mechanism of energy transformation of fast plasma flows into relativistic electrons and large amplitude magnetic fields is not known. The hypothesis of energy equipartition in a collisionless shock between the electrons, ions and magnetic fields has been shown in recent astrophysical models using large scale numerical simulations [A. Spitkovsky, 2008]. Laboratory experiments may provide further understanding of this obscure process. However, acceleration of sufficiently large volumes of matter to relativistic energies requires concentration of high densities of energy in a short time scale. Only high energy short pulse laser systems could be suitable for such experiments. The Target Normal Sheath Acceleration (TNSA, see Section 2) [Snavely et al., 2000; Wilks et al., 2001] can provide protons with energies of several tens of MeV corresponding to the streaming velocities of 20 – 30% of the velocity of light. The number of fast ions produced in one shot exceeds 10^{12}, which should be sufficient for the collective processes to become significant. The range of such protons is of the order of 1 g/cm^2, so the collisional effects should not be significant for distances of many ion inertia length, which define the characteristic thickness of the shock front.

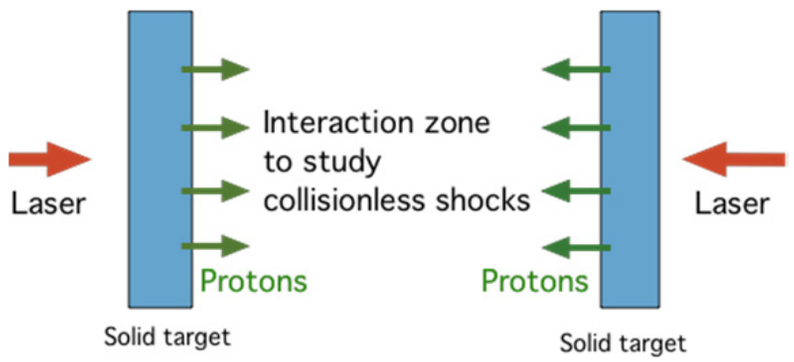


Figure 13. Schematic of the experimental setup required to perform the experiments discussed in this Section.

It was theoretically predicted that collisionless shocks may occur at mildly relativistic streaming velocities with a fraction ~ 10^{-4} of the total energy converted into magnetic field unless the electrons are heated significantly [Kato et al., 2008]. Experiments with non-relativistic laser pulses of sub-nanosecond duration and energy of a few hundred joules demonstrate a possibility of plasma streams formation with high Mach numbers, but the plasma temperature is relatively low and the ion mean free path remains shorter or comparable to the shock front thickness [Kuramitsu et al., 2011; Davis et al., 2010]. In a previous paper [S. Davis et al., 2010] it was proposed to collide the TNSA accelerated ion bunch with appropriately chosen low density plasma so the collective effects will dominate the ion stopping. [S. Davis et al. 2012] is dedicated to a more detailed study of electron heating and magnetic field generation in the overlapping region of the colliding plasmas: the first stage of formation of a collisionless shock. The characteristics of the high

energy proton bunch were optimized in large scale PIC simulations. The ions were accelerated from an overdense target to sub-relativistic velocities by the TNSA mechanism. The plasma instabilities are excited by the streaming ions. The overall interaction time of about one ion plasma period, $\omega_{pi}t_{max} \sim 6$, is not sufficient for excitation of ion instabilities and full shock formation. In this time interval one can see the development of electron instabilities, magnetic field generation and electron heating.

This study has allowed to show that during the beginning of the plasma collision, a strong electron heating is generated by a Weibel type filamentation and each ions beam is then slowed. The energy partition between ions, electrons and electromagnetic fields, at the foundation of astrophysical models of gamma-ray bursts was therefore studied and has allowed to have a better understanding of the mechanisms at play. The better knowledge of laser ion acceleration described in the other sections of this chapter allow to envision collisions with even higher velocities with more energetic lasers (see Section 5.2). This would allow to get closer to relativistic shocks and study other types of astrophysical shocks (pulsar winds, other types of shocks involved in gamma-ray bursts…). Using an external magnetic field, it will be possible to study shocks with different magnetizations (ratio of the magnetic energy density and of the kinetic energy density) and thus to study in the lab for the first time collisionless shocks with parameters similar to the ones in supernovae remnants (SNRs).

7. Conclusions and perspectives

Laser acceleration of intense, collimated and multi-MeV ion beams is a recent research domain, rising fast. Its advent has been made possible thanks to short pulse lasers with extremely high intensities and progresses at the fast pace of the development of these lasers. Because of its pulsed nature (the duration of the source is of the order of a few ps), its high beam quality, of the high number of produced ions (10^{11}-10^{13}), of the possibility to modulate the spectrum as well as the divergence of the beam, the ion source produced by laser appears useful and promising for a number of applications. One can quote high temporal and spatial resolution radiography, fast ignition, production of warm dense matter and, later on, high intensity injectors for accelerators and sources for protontherapy or radio-isotope production.

This chapter presents several important contributions to the domain of laser ion acceleration and its applications. These contributions, experimental, theoretical and numerical, cover the possibilities to obtain in various regimes compact ion accelerators both with existing high intensity lasers and with future laser systems. Several promising applications are detailed, as well as some of the necessary developments to obtain these results. It is shown that the TNSA mechanism is robust and used for existing applications and that the transparency regime and low density laser ion acceleration could be used for applications requiring high ion energies.

The applicability perspectives offered by these beams are interesting and will be pushed further, in particular thanks to the progresses that can be anticipated for the lasers and the

close opening of new installations like ILE, Gemini (at RAL), and further in time Apollon, ELI and diode pumped lasers with very high repetition rate and high energy. Thanks to these installations, it will be possible to increase the maximum energy and the dose of the ions (i) either by extrapolating simply using the mechanisms known nowadays, (ii) or by using other mechanisms (predicted or to be discovered) that will be more efficient.

To do so, the understanding of the accelerating parameters and the optimization of the laser parameters need to improved, by coupling theory and experiments, in order to obtain proton beams of a few hundred MeV, reproducible, controllable and predictable. This will require in particular to explore the scaling laws of existing mechanisms and to test the various mechanisms supposed to take place at ultra-high intensities 10^{21}-10^{22} W/cm^2 or higher (acceleration at the back surface, direct acceleration by the ponderomotive force, acceleration by electrostatic shock, acceleration by radiation pressure).

Future installations will possess various « lines », coupling laser pulses with similar intensities but with very variable durations ultra-short (10 fs) or moderately short (500 fs or more), which will offer the possibility to couple interaction regimes that are different, or even separated, and to take advantage of this coupling. For instance, the adjunction of bright X-ray sources and high energy proton sources will allow to probe dense plasmas heated by the protons. The proton sources will also be used to probe electron acceleration mechanisms. On these installations, it will be important to be able to change the parameters (pulse duration, energy, focalization) because if some applications require an excellent emittance, for others on the other hand the priority will go to ultra high energies (GeV and beyond), or to a maximum number of well collimated ions at low energy, different characteristics that require different ranges of laser parameters.

The progresses mentioned, the increase of energy in particular, should also open the way, as already mentioned, to new applicability perspectives, like injectors for high energy accelerators, the physics of ion beams (injection of multi-charged ion beams in matter), pulsed neutron sources, or even medical applications as well as material spallation and transmutation. Ultra high laser intensities (> 10^{24} W/cm^2) will even allow to test laser wakefield acceleration concepts, that are nowadays limited to electrons [Tajima and Dawson, 1979], with ions.

An intense international competition is underway both on the modeling of new acceleration regimes and on the experimental validation of these regimes. The recent results obtained at Los Alamos National Laboratory using some of the results presented in this chapter are an important illustration of this.

Author details

Emmanuel d'Humières
Université de Bordeaux – CEA - CNRS - CELIA, France

Acknowledgement

The author would like to thank Prof. V. T. Tikhonchuk, Prof. Y. Sentoku and Dr. J. Fuchs for fruitful discussions.

8. References

Adam J.C. et al. (2006), Phys. Rev. Lett. 97, 205006.
Albertazzi B. et al. (2012), submitted to Eur. Phys. J. Web of Conf.
Albright B.J. et al. (2007), Phys. Plasmas 14, 094502.
Allen M. et al. (2004), Phys. Rev. Lett. 93, 265004.
Alfvèn, H. (1939). On the Motion of Cosmic Rays in Interstellar Space, Phys. Rev. 55, 425.
Andresen G. B. et al. (2007), Phys. Rev. Lett. 98, 023402.
Antici P. et al. (2007), Phys. Plasmas 14, 030701.
Antici P. et al. (2008a), Phys. Rev. Lett. 101, 105004.
Antici P. et al. (2008b), J. Appl. Phys. 104, 124901.
Antici P. et al. (2009), New J. Phys. 11, 023038.
Atzeni S. et al. (2002), Nucl. Fusion 42, L1.
Begay F. et al. (1982), Phys. Fluids 25, 1675.
Bin J. H. et al. (2009), Phys Plasmas, 16, 043109.
Blanchot N. et al. (2008), Plasma Phys. Control. Fusion 50, 124045.
Borghesi M. *et al. (2002)*, Phys. Plasmas 9, 2214.
Borghesi M. et al. (2004), Phys. Rev. Lett. 92, 055003.
Borghesi M. et al. (2006), Fusion Science and Technology 49, 412.
Brunel F. (1987), Phys. Rev. Lett. 59, 52.
Buffechoux S., *et al. (2010),* Phys. Rev. Lett. 105, 015005.
Bulanov S. V. et al. (2002a), Plasma Physics Reports 28, 453.
Bulanov S. V. et. al. (2002b), Physics Letters A 299, 240.
Bulanov S. V. et al. (2007), Phys. Rev. Lett. 98, 049503.
Bulanov S. V. (2009), Plasma Phys. Control. Fusion 48, B29.
Capdessus R. et al. (2012), submitted to Phys. Rev. E.
Carrié M. et al. (2011), High Energy Density Physics 7, 353.
Ceccotti T. et al. (2007), Phys. Rev. Lett. 99, 185002.
Chen Z. L. et al. (2005), Phys. Rev. E 71, 036403.
Chen H. et al. (2009), Phys. Rev. Lett. 102, 105001.
Chen H. *et al. (2010),* Phys. Rev. Lett. 105, 015003.
Chen M. et al. (2011), Plasma Phys. Control. Fusion 53, 014004.
Chen S. et al. (2012), Phys. Rev. Lett. 108, 055001.
Clark E. et al. (2000a), Phys. Rev. Lett. 84, 670.
Clark E. et al. (2000b), Phys. Rev. Lett. 85, 1654.
Cowan T. et al. (2002), AIP Conference Proceedings 647, 135.
Cowan T. et al. (2004), Phys. Rev. Lett. 92, 204801.
d'Humières E. et al. (2005), Phys. Plasmas 12, 062704.

d'Humieres E. et al (2006), AIP Conference Proceedings 877, pp. 41-50.
d'Humières E. et al. (2007), Chinese Optics Letters, Vol. 5, Supplement, S136.
d'Humières E. et al. (2010a), J. Phys.: Conf. Ser. 244, 042023.
d'Humières E. et al. (2010b), AIP Conf. Proc. 1299, 704.
d'Humières E. et al. (2011a), MOP153, PAC11 proceedings.
d'Humières E. et al. (2011b), Eur. Conf. Abstracts 35G, P5.005.
d'Humières E. et al. (2012), submitted to Eur. Phys. J. Web of Conf.
Davis S. et al. (2010), Journal of Physics: Conference Series 244, 042006.
Davis S. et al. (2012), submitted to Eur. Phys. J. Web of Conf.
Debayle A. et al. (2010), Phys. Rev. E 82, 036405.
Denavit J. (1992), Phys. Rev. Lett. 69, 3052.
Disdier L. et al. (1999), Phys. Rev. Lett. 82, 1454.
Dong Q. et al. (2003), Phys. Rev. E 68, 026408.
Doumy G. et al. (2004), Phys. Rev. E 69, 026402.
Esirkepov T. Zh. et al. (1999), JETP Lett. 70, 82.
Esirkepov T. et al. (2006), Phys. Rev. Lett. 96, 105001.
Estabrook K. et al. (1978), Phys. Rev. Lett. 40, 42.
Fews A. et al. (1994), Phys. Rev. Lett. 73, 1801.
Flippo K. et al. (2008), Physics of Plasmas 15, 056709.
Flippo K. et al. (2010), J. Phys. Conf. Ser. 244, 022033.
Fourkal E. et al. (2002), Medical Physics 29, 2788.
Fritzler S. *et al. (2003)*, Appl. Phys. Lett. 83, 3039.
Fuchs J. *et al. (1999)*, Phys. Plasmas 6, 2569.
Fuchs J. et al. (2003), Phys. Rev. Lett. 91, 255002.
Fuchs J. et al. (2005), Phys. Rev. Lett. 94, 045004.
Fuchs J. et al. (2006), Nature Physics 2, 48-54.
Fuchs J. et al. (2007a), Phys. Plasmas 14, 053105.
Fuchs J. *et al*. (2007b), Phys. Rev. Lett. 99, 015002.
Fuchs J. et al. (2009), C. R. Physique 10, 176–187.
Gauthier M. et al. (2012), 39th EPS Conference on Plasma Physics proceedings – Stockholm, Sweden.
Gaillard S. et al. (2011), Phys. Plasmas 18, 056710.
Gitomer S. et al. (1986), Phys. Fluids 29, 2679.
Grech M. et al. (2011), *New J. Phys.* 13 123003.
Grismayer T. et al. (2006), Phys. Plasmas 13, 032103.
Gurevich A. V. et al. (1966), Sov. Phys. JETP 22, 449.
Habara H. *et al. (2004)*, Phys. Rev. E 70, 046414.
Haberberger D. et al. (2011), Nature Physics 7, 2130.
Hatchett S. *et al. (2000)*, Phys. Plasmas 7, 2076.
Hegelich B. M. et al. (2006), Nature 439, 441.
Henig A. et al. (2009), Phys. Rev. Lett. 103, 245003.
Jung D. (2012), Ph.D. dissertation – Ludwig Maximilians Universität München, Ion acceleration from relativistic laser nano-target interaction.

Kaluza M. et al. (2004), Phys. Rev. Lett. 93, 045003.
Kar S. et al. (2009), Phys. Rev. Lett. 102, 055001.
Kar S. et al. (2011), Phys. Rev. Lett 106, 225003.
Kato T. et al. (2008), Astrophys. J. 681, L93.
Key M. et al. (2006), Fusion Science and Technology 49, 440.
Klimo O. et al. (2008), Phys. Rev. Special Topics-Accelerators And Beams, 11(3):031301.
Klimo O. et al. (2011), New J. Phys. 13, 053028.
Kodama R. *et al*. (2004), Nature 432, 1005.
Krushelnick K. et al. (1999), Phys. Rev. Lett. 83,737.
Krushelnick K. et. al. (2000), IEEE Trans. Plasma Sci 28, 1184.
Kuramitsu Y. et al. (2011), Phys. Rev. Lett. 106, 175002.
Lancaster K. et al. (2007), Phys. Rev. Lett. 98, 125002.
Ledingham K.W. D. et al. (2004), J. Phys. D: Appl. Phys. 37 2341.
Leemans W. et al. (2006) Nat. Phys. 2, 696.
Lefebvre E. et al. (1997), Phys. Rev. E 55, 1011.
Lefebvre E. et al. (2006), J. of App. Phys. 100, 113308.
Limpouch J. et al. (2008), Laser & Part. Beams 26, 225.
Macchi A. et al. (2009), Phys. Rev. Lett. 103, 085003.
Mackinnon A.J. *et al. (2002)*, Phys. Rev. Lett. 88, 215006.
Mackinnon A.J. et al. (2004), Rev. Sci. Inst. 75, 3531.
Malka G. *et al. (1996)*, Phys. Rev. Lett. 77, 75.
Malka V. et. al. (2004), Medical Physics 31, 1587.
Malka V. (2008), Principles and applications of compact laser–plasma accelerators, Nature Physics 4, 447-453.
Maksimchuk A. et al. (2000), Phys. Rev. Lett. 84, 4108.
Mancic A. *et al. (2010a),* High Energy Density Physics 6, 21.
Mancic A. et al. (2010b), Phys. Rev. Lett. 104, 035002.
Mora P. (2003), Phys. Rev. Lett. 90, 185002.
Mora P. (2005), Phys. Rev. E 72, 056401.
Mourou G. et al. (2006), Rev. Modern Phys. 78, 309.
Murakami Y. et al. (2001), Phys. Plasmas 8, 4138.
Nakamura T. et al. (2004), Phys. Rev. Lett. 93, 265002.
Nakamura T. et al. (2007), Phys. Plasma 14, 103105.
Nakatsutsumi M. et al. (2007), Phys. Plasma 14, 050701.
Nakatsutsumi M. et al. (2008), J. of Physics: Conf. Series 112, 022063.
Naumova N. et al. (2009), Phys. Rev. Lett. 102, 025002.
Neely D. et al. (2006), App. Phys. Lett 89, 021502.
Nemoto K. et al. (2001), Appl. Phys. Lett. 78, 595.
Offermann D.T. et al. (2011), Phys. Plasmas 18, 056713.
Palmer C.A. et al. (2011), Phys. Rev. Lett. 106, 014801.
Patel P. et al. (2003), Phys. Rev. Lett. 91, 125004.
Peano F. et al. (2007), Phys. Plasmas 14, 056704.
Pelka A. et al. (2010), Phys. Rev. Lett. 105, 265701.

Perez F.et al. (2010a), Phys. Rev. Lett. 104, 085001.
Perez F. et al. (2010b), Phys. Plasmas 17, 113106.
Pommier L. et al. (2003), Laser Part. Beams 21, 573.
Popescu H. *et al. (2005)*, Phys. Plasmas 12, 063106.
Psikal J. et al. (2008), Phys. Plasmas 15, 053102.
Psikal J. et al. (2010), Phys. Plasmas 17, 013102.
Pukhov A. (2001), Phys. Rev. Lett. 86, 3562.
Quéré F. et al. (2006), Phys. Rev. Lett. 96, 125004.
Renard-Le Galloudec N. et al. (2008), Rev. Sci. Inst. 79, 083506.
Renard-Le Galloudec N. et al. (2009), Phys. Rev. Lett 102, 205003.
Renard-Le Galloudec N. et al. (2010), Laser and Particle Beams 28, 513.
Robinson A. P. L. et al. (2007), Phys. Plasmas 14, 083105.
Robinson A. P. L. et al. (2008), New Journal Of Physics, 10:013021.
Robson L. et al. (2007), Nat. Phys. 3, 58.
Romagnani L. *et al*. (2005), Phys. Rev. Lett. 95, 195001.
Roth M. et al. (2001), Phys. Rev. Lett. 86, 436.
Roth M. *et al*. (2002), Phys Rev ST-AB 5, 061002.
Ruhl H. et al. (2001), Plasma Phys. Report, 27, 5, 363-371.
Ruhl H. et al. (2004), Phys. Plasmas 11, L17.
Sack C. et al. (1987), Physics Reports 156, 311.
Santala M. et al. (2000), Phys. Rev. Lett. 84, 1459.
Santala M. et al. (2001), Appl. Phys. Lett. 78, 19.
Sarkisov G. S. et al. (1999), Phys. Rev. E 59, 7042.
Schirber M. et al. (2005), Science 310, 1610-1611.
Schlegel T. et al (2009)., Phys. Plasmas 16, 081303.
Schollmeier M. et al. (2011), Bull. Am. Phys. Soc.
http://meetings.aps.org/link/BAPS.2011.DPP.NO7.1.
Schwoerer H. et al. (2006), Nature 439, 445.
Sentoku Y. (2000) et al., Phys. Rev. E 62, 7271.
Sentoku Y. et al. (2003a), Phys. Plasmas 10, 2009.
Sentoku Y. et al. (2003b), Phys. Rev. Lett. 90, 155001.
Sentoku Y. et al. (2004), Phys. Plasmas, 11, 3083.
Sentoku Y. et al. (2008), J. Comput. Phys. 227, 6846.
Sentoku Y. et al. (2011), Phys. Rev. Lett. 107, 135005.
Silva L. et al. (2004), *Phys. Rev. Lett.* 92, 015002.
Snavely R. et al. (2000), Phys. Rev. Lett. 85, 2945.
Snavely R. et al. (2007), Phys. Plasmas, 14, 092703.
Sokolov I. V. (2009a), Journ. Exp. Theor. Phys. 109, 207.
Sokolov I.V. et al. (2009b), Phys. Plasmas 16, 093115.
Sokolov I.V. et al. (2010), Phys. Rev. E 81, 036412.
Sokolov I. V. et al. (2011), Phys. Plasmas 18, 093109.
Solodov A.A. et al. (2009), Phys. Plasmas 16, 056309.
Solodov A. A. et al. (2010), J. Phys. Conf. Series 244, 022063.

Spitkovsky A. (2008), Astrophys. J. 673, L39.
Stephens R. et al. (2004), Phys. Rev. E 69, 066414.
Storm M. et al. (2009), Phys. Rev. Lett. 102, 235004.
Tabak M. et al. (1994), Phys. Plasmas 1, 1626.
Tabak M. et al. (2006), Fusion Sci. and Tech. 49, 254.
Tajima T. and Dawson J. (1979), Phys. Rev. Lett. 43, 267–270.
Tamburini, M. et al. (2010), New Journ. Physics 12 123005.
Tamburini M. et al. (2012), Phys. Rev. E 85, 016407.
Temporal M. et al. (2002), Phys. Plasmas 9, 3098.
Temporal M. (2006), Phys. Plasmas 13, 122704.
Tikhonchuk V.T. et al. (2005), Plasma Phys. and Control. Fusion 47, 869.
Toncian T. et al. (2006), Science 312, 410.
Weibel E.S. (1959), Phys. Rev. Lett. 2, 83.
Wilks S. et al. (1992), Phys. Rev. Lett. 69, 1383.
Wilks S.C. (1993), *Simulations of ultraintense laser-plasma interactions,* Phys Fluids B 5, 2603.
Wilks S. C. et al. (2001), Phys. Plasmas 8, 542.
Willingale L. et al. (2006), Phys. Rev. Lett. 96, 245002.
Willingale L. et al. (2007), Phys. Rev. Lett. 98, 049504.
Willingale L. et al. (2009), Phys. Rev. Lett. 102, 125002.
Wittmann T. et al. (2006), Rev. Sci. Instrum. 77, 083109.
Yamagiwa M. et al. (1999), Phys. Rev. E 60, 5987.
Yang J. M. et al. (2004), J. Appl. Phys. 96, 6912.
Yin L. et al. (2006), Laser and Particle Beams 24, 291.
Yogo A. et al. (2008), Phys. Rev. E 77, 016401.
Youssef A. et al. (2006), Phys. Plasmas 13, 030702.

IntechOpen